Spring 2023

Mathematical Analysis of Electrochemical Systems

Shiv Krishna Reddy Madi Reddy

Mathematical Analysis of Electrochemical Systems

By

Shiv Krishna Reddy Madi Reddy

Bachelor of Science
Indian Institute of Technology, Varanasi 2015

Master of Science
University at Buffalo - SUNY 2018

Submitted in Partial Fulfillment of the Requirements

for the Degree of Doctor of Philosophy in

Chemical Engineering

College of Engineering and Computing

University of South Carolina

2023

Accepted by:

Ralph E. White, Major Professor

Melissa A. Moss, Committee Member

William E. Mustain, Committee Member

Edward P. Gatzke, Committee Member

Xingjian Xue, Committee Member

Cheryl L. Addy, Interim Vice Provost and Dean of the Graduate School

Abstract

A solid electrolyte interphase (SEI) growth model is developed in a mixed mode that contains solvent diffusion through the SEI layer and corresponding solvent reduction kinetics at the SEI/electrode interface. The governing equations are solved by the Landau transformation, which makes the moving layer fixed to predict the open circuit potential, SEI layer thickness, and capacity loss. The estimated parameters fitted with experimental data from the literature are computed using COMSOL and MATLAB. Results show that the mixed mode model predicts lower capacity loss and thinner SEI layer due to its growth under open circuit conditions than previously reported by others.

A short-time asymptotic analysis is performed to establish corrections of the Ilkovich equation, which describes the polarographic response of a dropping mercury electrode. The convective-diffusion equation governing diffusion-limited reactant flux for small drop times is solved by a regular perturbation based on powers of the sixth root of time. This produces a framework within which higher terms of the Ilkovich equation can be derived systematically. As well as reproducing Ilkovich's original formula and verifying Newman's correction of Koutecky's first-order term, we calculate the second-order term for the first time. The calculation is compared to the Newman–Levich procedure and tested against numerical simulations with finite-element software.

A method is presented which can be used to obtain analytical solutions for boundary value problems (BVPs) using the matrix exponential and Maple. Systems of second order, linear differential equations are expressed as two or more first order

equations in matrix form, and their solutions are obtained using the matrix exponential, matrix integration, and matrix inverse methods using Maple. The solution process is illustrated for single and multiple domains with different types of boundary conditions and constraints when necessary due to the boundary conditions. The method is easier to use and could be extended to include partial differential equations (PDEs).

Contents

List of Tables

List of Figures

Chapter 1

Introduction

Lithium-ion batteries have been gaining significant popularity in recent years. As a result, the market is expected to grow from USD 44.5 billion in 2022 to USD 135.1 billion by 2031, at a compound annual growth rate (CAGR) of 13.1% [1]. One of the major sectors contributing to this growth is the transportation sector, thanks to the popularization of electric vehicles. Plug-in electric vehicles (PEVs) have been considered by many as the most promising choice to replace conventional internal combustion engine vehicles due to their energy and environmental implications. In addition to having a lower operational cost due to cheap electricity, they could address the transportation sector's environmental and energy challenges by reducing fossil fuel consumption and greenhouse gas and pollutant emission.

The penetration of PEVs is limited by some major concerns related to the safety and performance of the Li-ion battery system. These issues include the risk of fire and explosion, range anxiety due to unpredicted battery depletion, an unsatisfactory lifetime, etc. Therefore, a battery management system (BMS) capable of advanced battery control and diagnostics, like real-time state estimation, charging control, thermal management, etc., is the key to addressing these issues, and the basis of such a BMS system is accurate battery models.

1.1 Background on Lithium-ion Batteries

A Lithium-ion battery is a rechargeable electrochemical cell that produces electric current from internal chemical reactions. It consists of a positive and a negative elec-

trode, a separator, and electrolyte, as shown in the schematic in Fig. 1.1. Both of these electrodes contain active materials that store lithium ions. The active material in the positive electrode is generally made of lithium metal oxide, or $LiMO2$, where M stands for a metal element like Cobalt or Manganese or a combination of metal elements like Nickel and Manganese. The active material in the negative electrode is mostly carbon C, which can be lithiated to store lithium during charging. Additionally, the electrodes contain binder material that binds the active materials and keep them in contact with the current collectors and additives such as carbon black for cathode to increase its conductivity. The electrolyte provides a medium for the Li-ion to migrate from one electrode to another through the separator. The separator allows the transport of Li-ion while restricting the migration of electrons, thus forcing them to flow through the external circuit.

A fully charged Li-ion battery contains all the cyclable Li-ions at the anode. During discharge, Li-ions and electrons are created at the surface of the anode particles by an electrochemieal reaction,

$$Li_xC_6 \rightleftharpoons C_6 + xLi^+ + xe^- \tag{1.1}$$

These Li-ions flow from anode to cathode through the electrolyte across the separator while the corresponding electrons flow through the external circuit and reach the positive electrode. This flow of ions is governed by the electrical potential difference and the ionic concentration gradient between the two electrodes. Moreover, the loss of ions at the surface of the anode particle during discharge is replenished by the diffusion of ions from the particle core to the surface.

The ions from anode during discharge and their corresponding electrons react at the surface of the cathode particle to produce Lithium metal oxide such as $LiCoO2$. This reaction is given by,

$$Li_{1-x}CoO_2 + xLi^+ + xe^- \rightleftharpoons LiCoO_2 \tag{1.2}$$

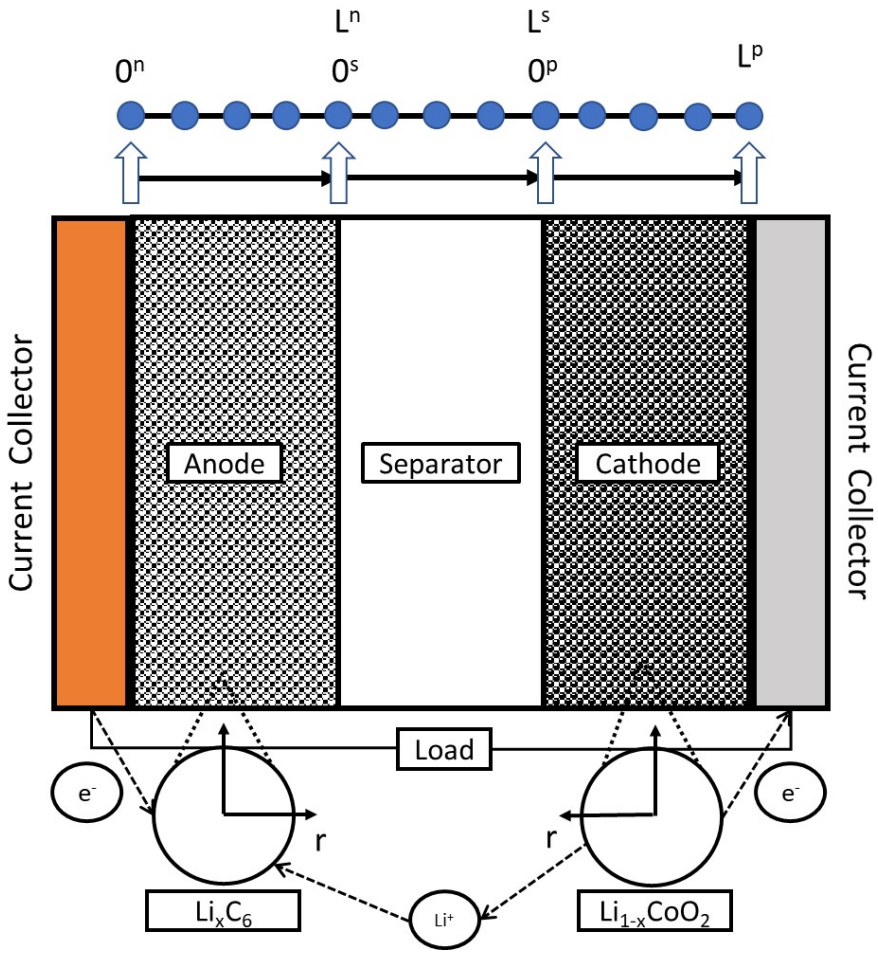

Figure 1.1: Schematic of the Doyle-Fuller-Newman model. The model considers two phases: the solid and the electrolyte. In the solid, states evolve in the x and r dimensions. In the electrolyte, states evolve in the x dimension only. The cell is divided into three regions: anode, separator, and cathode.

A fully discharged battery will contain all the cyclable ions at the cathode and the entire process is reversed during charging.

1.2 Research Outline

The dissertation is organized as follows:

In chapter 2, a SEI Growth model is presented for the Open-Circuit Conditions. SEI growth and capacity loss for a mixed mode model, where diffusion of the solvent through the SEI layer is combined with a solvent reduction reaction at the

SEI/electrode interface is presented. In Chapter 3, a perturbation method is used to develop a second-order correction to the Ilkovich equation. We show that the instantaneous molar flowrate $N(t)$ of a solute with bulk concentration c_∞ and diffusivity D at the surface of a dropping mercury electrode supplied at volumetric flowrate Q depends on time t. Chapter 4 presents efficient mathematical methods for solving chemical and electrochemical systems. Finally, the method is used to obtain a solution for a lithium/polymer cell model.

Chapter 2

Mathematical Model for SEI Growth under Open-Circuit Conditions

2.1 Introduction

Capacity fade occurs during storage of lithium-ion battery cells. Several processes cause this capacity loss of lithium-ion batteries, including loss of active electrode material, loss of cyclable lithium ions and electrolyte decomposition due to parasitic electrochemical reactions on the electrode surface [2, 3]. The growth of solid electrolyte interface (SEI), which is a product from the parasitic reactions, inhibits further electrolyte decomposition [4]. In the literature, many researchers have investigated the most important lithium-ion battery degradation mechanism is the growth of the SEI layer on the graphite electrode [5, 6, 7, 8, 9, 10, 11, 12, 13, 14, 15, 16, 17, 18, 19, 20, 21, 22, 23, 24, 25, 26, 27, 28, 29, 30, 31, 32, 33, 34, 35, 36, 37, 38, 39, 40, 41]. In these studies, the SEI growth was modeled by assuming either kinetically limited [18, 24, 25, 29], transport limited [21, 32, 42] or electron tunneling [36, 37, 38].

In the parabolic SEI growth models developed by Peled et al.,[4] and Broussely et al.,[6] they assumed that electron transport across the SEI layer is the rate-determining step. The side reactions were assumed to occur on the interface between the SEI layer and electrolyte. However, they did not validate their equations against any SEI experimental measurements. Christensen et al.[7], Colclasure et al.[8], Das et al.,[36], and Tang et al.[37] developed mixed mode models based on the diffusion of electrons across SEI. Also, these authors did not support their hypothesis of elec-

trons transfer across the SEI layer with any SEI experimental data in all these studies [7, 8, 41].

Das et al.[36] proposed a mixed ion electron conductor SEI growth model with spatially resolved concentrations. In their work, they assume that electron transport is rate limiting as opposed to solvent diffusion and the source of lithium ions participating in SEI growth is the electrolyte. Their assumption may be valid for short periods of storage time, but they do not present any experimental evidence to support their assumptions. We think the diffusion of solvent can explain their observations. Chouchane et al.[35] reported a new 3D microstructure resolved computational model, and the exponential dependence of SEI growth on electrode potential led to inhomogeneous SEI growth throughout the electrode. In our model, we focused on a local scale at the electrode/electrolyte interface by simplifying the actual porous electrode mesostructure, which we described by using an effective diffusivity in porous media.

SEIs formed on Li, Na, and Mg metal electrodes have received increased attention from the scientific research community. For example, Lim et al.[43] reported that densification of SEI is observed on Li/Na metal electrodes in carbonate electrolytes and glyme-based electrolytes. Furthermore, the gradual change of overpotential is shown during cycling on Li metal, whereas Na exhibits intermittent overpotential spikes, which may lead to chemical/ mechanical instabilities. Also, on Mg metal electrodes with glyme-based electrolytes, the surface limiting reaction growth mechanism is shown to proceed through SEI densification or because of inherent mechanical instabilities [44].

Zhang et al.[33] developed a single particle model to simulate the loss of lithium ions and listed various stages of capacity fade during the constant voltage conditions. They calibrated against experimental data to obtain estimated parameters and proposed that the first stage of capacity loss is relevant with SEI. Ning et al.[18], Ramadass et al.[24], developed a charge-discharge cycling model to simulate the ca-

pacity fade of Li-ion batteries by considering the kinetics of the solvent reduction reaction.

Capacity fade as a function of time raised to half, $t^{0.5}$, is most commonly attributed to diffusion limited SEI growth models for lithium-ion batteries [21, 28, 41]. Ploehn et al.[21] proposed an SEI formation model by considering the solvent diffusion through the SEI porous layer as the rate-determining step, and the numerical results match the experimental observations reasonably well. Yoshida et al.[32] measured the SEI thickness on the anode carbon surface by focused ion beam (FIB), scanning electron microscopy (SEM), and X-ray photoelectron spectroscopy (XPS). They assumed that SEI is formed by a reaction between intercalated Li and the electrolyte in the SEI on the negative carbon surface where diffusion of the electrolyte in the SEI is the rate-determining step of the reaction. Furthermore, these authors assumed that the electrons are located on the carbon surface, and the SEI is an ionic conducting and electronically insulating layer.

Sankarasubramanian et al.[28] assumed linear diffusion of the solvent through the SEI layer and used first order kinetics to describe side reactions. Deshpande et al.[10] extended Phul et al.s[19] work by adding the diffusion of the solvent, but the results did not match with the experimental data. Pinson et al.[20] used first-order kinetics and linear diffusion of solvent through SEI to express a side reaction in the single-particle model. The loss of lithium is used to show the formation of SEI on the negative electrode. They applied Butler-Volmer kinetics and charged species conservation as an alternative way to describe the side reaction and simulated the SEI layer growth in the porous electrode model.

Lamorgese et al.[14], Ashwin et al.[5], Fu et al.[11], and Lin et al.[16] set up a pseudo-two-dimensional (P2D) model to simulate the SEI formation by applying porous electrode theory and assuming that the current density of the side reaction which follows Tafel kinetics. Liu et al.[17] and Zhao et al.[34] added the solvent

diffusion which follows Ficks second law through the SEI layer in their P2D simulation. Jin et al.[12] used a reduced-order approach to simplify the P2D model which contains solvent diffusion and Tafel kinetics, and they were able to validate their model with the experimental results. Kamyab et al.[13] extended Ploehn et al.[21] work by adding the Tafel kinetics within the film growth to mixed mode. They also assumed the linear diffusion problem but with Tafel kinetics to obtain an analytical solution of SEI films thickness and capacity loss to compare with the experimental data under trickle charge storage. Rahamian et al.[23] listed the kinetic-limited and diffusion-limited processes under extreme conditions to reveal that the growth of SEI is linear in the kinetic-limited region initially, and then the thickness is a function of the square root of time in the diffusion-limited region. Safari et al.[27] in 2008 proposed the diffusion of solvent and Tafel kinetics in a single-particle model under various conditions. They concluded that the growth of the film would be controlled by diffusion; besides, under OCV storage, the values of the diffusion coefficient and reaction rate adjusted by them were relatively large. Safari et al.[26] in 2011 refined their equations and parameters to simulate their model again. They ignored the change of the open-circuit voltage and the influence of the initial SOC. After the improvement, they concluded that both diffusion and kinetics control the growth of the SEI film, and the growth of the film is maximized when the initial SOC is 100%.

The diffusion of a solvent through the film combined with the electrochemical kinetics of the side reaction will describe the film growth. Ramasamy et al.[25] simulated zero-dimensional SEI growth and capacity loss under open-circuit conditions using Tafel kinetics only; an ordinary differential equation is listed as how lithium is consumed in the side reaction. In this work, we extend their model by establishing a one-dimensional SEI film, the diffusion of the solvent in the film, which follows Ficks second law. The electrochemical reaction occurs at the interface between the SEI and the electrode. According to the theory of moving SEI film mentioned by Kamyab et

al.[13] and Ploehn et al.[21], the growth rate of SEI is obtained.

All the previous models reviewed here focused on cycling effects, constant voltage charging. We present here a mixed mode model operated under open circuit conditions, where diffusion of the solvent through the SEI layer is combined with a solvent reduction reaction at the SEI/electrode interface. The governing equations are solved numerically using COMSOL and MATLAB to predict the OCV value of the electrode, the SEI layer thickness, and the capacity loss. The OCV of the negative electrode from the model is fitted with the experimental data obtained from a SONY 18650 lithium-ion cell [25]. The effective diffusion coefficient of the solvent and the kinetic reaction rate of the SEI side reaction are obtained from curve fitting with the experimental data. Additionally, we developed an alternative approach to solve the nonlinear partial differential equation using the Landau transformation. By making the moving boundary fixed, we can solve the governing equations and boundary conditions easily and optimize the best-estimated parameters.

2.2 Model Development

System geometry and physical assumptions

The solvent (S) and lithium ions (Li^+) diffuse through the SEI layer and react with the electrons on the electrode surface, which results in the formation of an insoluble product (P) at the electrode/SEI interface. The SEI growth on the electrode is shown schematically in Figure 2.1 In the present study, the model is developed to analyze the behavior of critical aging mechanisms and their impact on the capacity fade in the negative electrode. The following assumptions have been applied in the modeling of SEI growth under open circuit conditions.

1. Two components are in the system: porous domain of solvent (c_s) and lithium ions (Li^+) at the electrode surface.

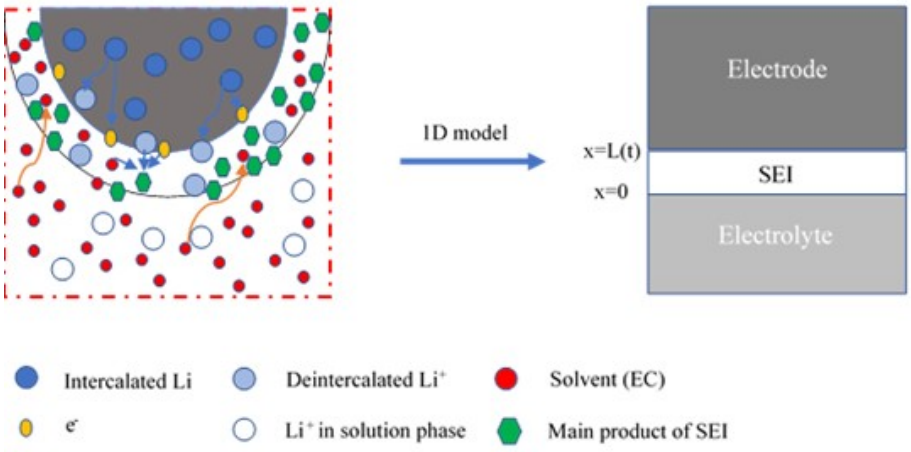

Figure 2.1: Schematic illustration of the side reaction at the anode particle. The solid lithium ions (blue circles) de-intercalate the solution lithium ions (grey circles) and electrons (yellow circles); the solvent (ethylene carbonate) (red circles) will react with electrons and lithium ions at the electrode surface, the product covers the surface of the electrode and increases with the storage time. The product is shown as green hexagons. The right schematic is a one-dimensional SEI layer which is the projection from the particle.

2. Decomposition of anion are not considered at the electrode/electrolyte interface as the electrolyte used was 1M $LiPF_6 - EC/PC$ (50:50 vol %) which is very dilute.

3. We assume a porous structure for the SEI layer, the liquid electrolyte fills the pores of the SEI and reaches the electrode surface.

4. Diffusion of the solvent occurs only in the x direction; thus, the growth of the SEI is uniform in the y and z directions.

5. The overall self-discharge rate is so slow that it is not limited by diffusion of lithium ions out of the carbon electrode.

Electrochemical SEI reaction kinetics

The electrochemical reaction for SEI formation at the solid/electrolyte interface can be expressed as [45, 46]:

$$2Li^+ + S + 2e^- \rightarrow P \tag{2.1}$$

A schematic of the electrode-SEI-electrolyte interface is shown in Figure 1. For an SEI layer much smaller in thickness than a typical particle of active material, the particle surface can be assumed to have zero curvature and is modeled in 1D cartesian coordinates. (P) represents the main inorganic component of solid electrolyte interphase (SEI). Christensen et al.[7] and Colclasure et al.[8] listed their reactions and utilized (Li_2CO_3) as the main product. The releasing of flammable hydrocarbon methane gas is ignored in this work for simplicity. The rate of SEI formation is obtained from the kinetic equation for the electrochemical reaction at the electrode surface based on the Butler-Volmer equation:

$$J_{SEI} = J_{SEI,0}\left[\frac{c_p}{c_{p,max}}\exp\left(\frac{\alpha_a nF\eta_{SEI}}{RT}\right) - \frac{c_s}{c_{s,max}}\frac{c_{Li}^2}{c_{Li,max}^2}\exp\left(-\frac{\alpha_c nF\eta_{SEI}}{RT}\right)\right] \tag{2.2}$$

In Eq. (2), the exchange current density for solvent reduction, , depends on the initial surface concentration of lithium ions.

$$J_{SEI,0} = nFk_{SEI}c_{Li,max}^{n(1-\alpha_c)} \tag{2.3}$$

where k_{SEI} is the kinetic reaction rate constant. We assumed that the potential window of interest is far from the reversible potential; consequently, it should be reasonable to model the SEI side reaction with Tafel kinetics [24, 25, 47] as follows:

$$J_{SEI} = -J_{SEI,0}\left[\frac{c_s}{c_{s,max}}\frac{c_{Li}^2}{c_{Li,max}^2}\exp\left(-\frac{\alpha_c nF\eta_{SEI}}{RT}\right)\right] \tag{2.4}$$

where c_s is the solvent concentration in the SEI porous layer. The overpotential η_{SEI} is defined as

$$\eta_{SEI} = U^{OCP} - U_s^{SEI} \tag{2.5}$$

where U^{OCP} is the open-circuit potential of the anode, which is a function of SoC, as given in Appendix C. U_s^{SEI} is the irreversible open circuit potential for solvent reduction, which is a constant. The side reaction consumes not only solvent but also active lithium ions. The consumption of lithium ions will be expressed by an ordinary differential equation since there is no net current. Therefore, the consumption of lithium is proportional to the current density of the side reaction.

$$\frac{1}{a}\frac{dc_{Li}}{dt} = \frac{J_{SEI}}{nF} \tag{2.6}$$

where a is a specific surface area whose value is listed in Table 1.

Solvent diffusion

Ficks second law obtains a linear diffusion equation representing the solvent diffusion in the SEI layer in a moving boundary system.

$$\frac{\partial c_s}{\partial t} = D_s^{eff}\frac{\partial^2 c_s}{\partial x^2} \tag{2.7}$$

where c_s is the concentration of the solvent and D_s^{eff} is the effective diffusivity of the solvent.

$$D_s^{eff} = D_s\epsilon_{SEI}^{1.5} \tag{2.8}$$

where D_s is the free stream diffusion coefficient of the solvent and is the SEI porosity. The above equation is valid in the region $x = 0$ to $x = L(t)$, where $L(t)$ represents the length of the SEI layer (SEI-electrode interface, see Figure 1). The corresponding initial and boundary conditions are as follows. At the interface between the SEI and the electrolyte, the concentration is given by

$$c_s = \epsilon_{SEI}c_{s,bulk} \quad @ \quad x = 0 \tag{2.9}$$

At the boundary between the SEI and the electrode, the solvent flux matches the side reaction current, which gives

$$-D_s^{eff}\frac{\partial c_s}{\partial x} = -\frac{J_{SEI}}{nF} \quad @ \quad x = L \tag{2.10}$$

where $c_{s,bulk}$ is the solvent concentration in the bulk of the electrolyte. Initially, the solvent concentration $c_s = \epsilon_{SEI} c_{s,bulk}$ in the SEI layer.

Surface film thickness

SEI layers constitute the surface film covering the graphite electrode. In the model, the growth rate of SEI will be associated with the flux at the electrode/SEI interface, which is derived by Kamyab et al.[13]

$$\frac{dL}{dt} = -D_s^{eff} \frac{M_p}{\rho_p} \frac{dc_s}{dx} \tag{2.11}$$

where M_p and ρ_p are molar weights and densities for the SEI layer. The ratio of the thickness to the molar weight corresponds to constant concentration for the SEI layer formed on negative electrodes, and they are given as c_p in Table 1.

Numerical solution technique

The mathematical model for the SEI growth under open-circuit conditions has two governing equations Eqs. (6) and (7), which need to be solved simultaneously. These nonlinear partial differential equations are coupled with changing the thickness of the system due to the formation of the SEI Eq. (11). This moving boundary problem can be transformed into a fixed boundary problem by introducing new space coordinates and applying the Landau transform. The transformations in the porous SEI medium $0 < x < L(t)$ is given by the following equation.

$$\xi = \frac{x}{L(t)} \tag{2.12}$$

where ξ is the dimensionless spatial positions in the SEI layer vary between 0 and 1. Applying this transformation results in a modification of the governing equations and boundary conditions. The change of coordinates and application of Landau transforms are described in Appendix D.

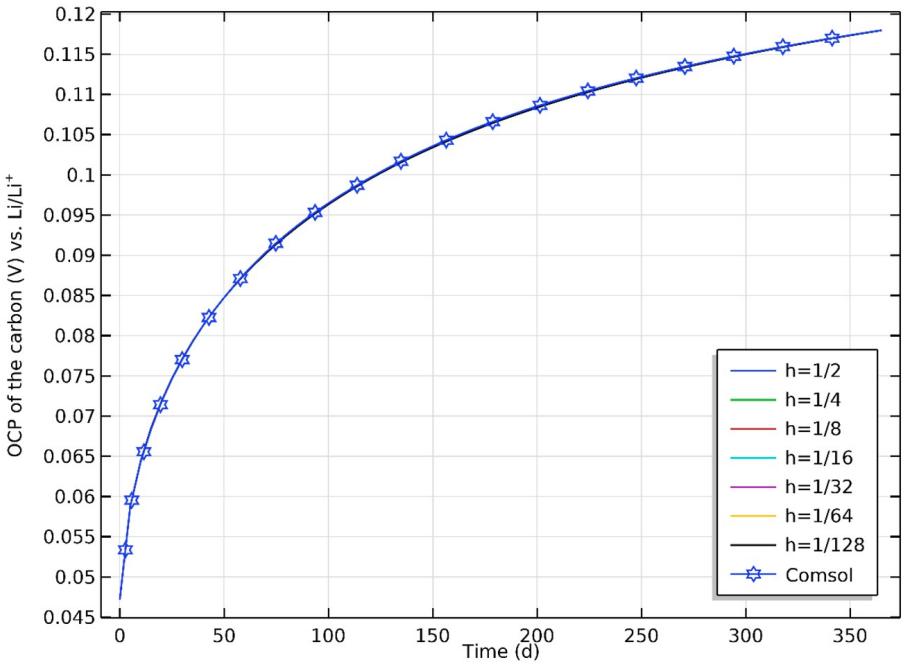

Figure 2.2: The OCP curves from solutions with different grid spacing h.

The modified equations were solved by using a commercial finite element package, COMSOL Multiphysics (version 5.6), and by using a fully implicit backward time centered space finite difference method in MATLAB. This converts the differential equations into nonlinear and linear equations, which were solved using MATLABs stiff solver ode 15s. The OCP versus time curves from solutions for decreasing values of the grid spacing, h, is presented in Figure 2. The results from both the methods are consistent. All the simulations in this paper were performed on a PC with a 3.80 GHz processor and 64 GB RAM (running Windows 10).

Parameter estimation

To check the agreement of the mathematical model with the experimental data obtained on the SONY 18650 lithium-ion cell, the values of certain parameters in this model need to be estimated. Parameter estimation is a useful approach to find kinetic and transport parameters from the experimental data. Therefore, we used two methods in this work: the optimization module in COMSOL and a multi-parameter

least square curve fitting procedure in MATLAB to interpret the data. Such techniques are typically formulated to minimize the sum-of-squared differences between the model outputs and their experimentally measured values.

$$Obj = min_p \left\{ \sum_{i=1}^{n} \left(OCP_i^{mod}(t_i, p) - OCP_i^{exp}(t_i) \right)^2 \right\} : p^l \leq p \leq p^u \tag{2.13}$$

where subscripts *mod* and *exp* represent model and experimental results, and p^l and p^u are the lower and upper bounds for the parameters, respectively; n represents the number of time steps simulated. The nonlinear regression is performed using the Levenberg-Marquardt optimization algorithm in COMSOL Multiphysics and the least squares subroutine in MATLAB (LSQNONLIN). Therefore, by fitting the OCP curves, two parameters are estimated simultaneously with 95% confidence intervals: the kinetic reaction rate constant of side reaction and the effective diffusion coefficient of solvent. Confidence intervals for individual parameters are determined using the t-test statistic and the linear approximation method[48] that specifies an upper and lower limit to the deviation from the optimal solution. The confidence interval for an individual parameter p_j for a confidence level $(1 - \alpha)$ is given by $p_j \pm t_{(1-\alpha/2,n-k)}\sigma_j$ where σ_j is the standard deviation of the parameter p_j, and k is the number of parameters to identify. Here $t_{(1-\alpha/2,n-k)}$ statistic has two arguments $n - k$ degrees of freedom, and that leaves a probability of $\alpha/2$ in the upper tail and $1 - \alpha/2$ in the lower tail.

2.3 Result and Discussion

Connection of model with experiment

The OCV of the SONY 18650 lithium-ion cell as a function of time at different temperatures of 25 °C and 35 °C is reported in the literature by Ramasamy et al [25]. Table I summarizes the design specifications and a list of characteristics of this cell. The OCP, SEI thickness, and capacity loss provide a better understanding of

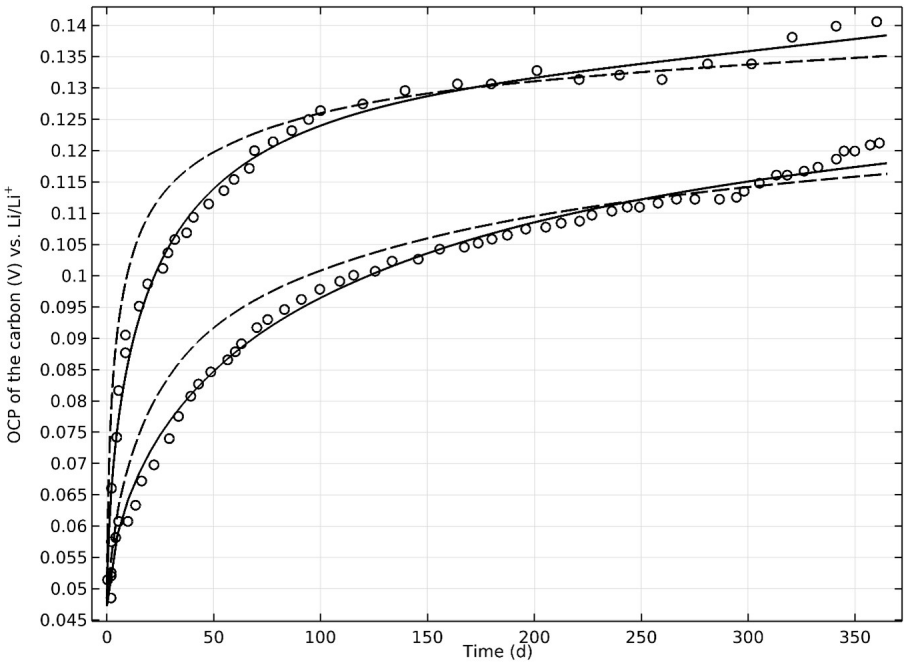

Figure 2.3: Data for the SONY 18650 cell stored at 100% SOC and were performed at 25 °C and 35 °C over 365 days (o). The lines are from the numerical solution of our mixed mode model (-) and kinetic limited model (- - -) for OCP of the negative electrode as a function of time in days.

how different parameters such as D_s^{eff}, k_{SEI}, and ϵ_{SEI} are correlated with each other to obtain a certain OCP value and how a variation may affect the output.

The OCV vs. t data points for the SONY 18650 cell and the mixed mode model fit is shown in Figure 3. The kinetic limited model by Ramasamy et al.[25] is reproduced by assuming that the SEI growth occurs at the kinetic limited rate (i.e., the concentration of the solvent is present in excess at the anode/SEI film interface). Ramasamy et al.[25] assumed the SEI layer to be a non-porous solid phase and predicted that the capacity loss caused by the SEI growth changes linearly with the square root of time. As shown in Figure 2.3 here and in Figure 3 in Ref. [24], in which they fit their kinetic limited model predictions to their experimental data, it can be seen that the kinetic-limited model is only an approximate model. Also, the kinetic rate constant extracted from their fit to the experimental data for 25 °C and 35 °C is one order of magnitude smaller and than the kinetic rate constant in our

Table 2.1: Published and assumed characteristics of the SONY 18650 lithium-ion cell.

Symbol (Unit)	Description	Value	References
a	Specific surface area of the electrode	3×10^6	[24]
$c_{Li,max}$	Maximum lithium concentration in the electrode	3.056×10^4	[24]
$c_{s,bulk}$	Bulk concentration of solvent	4541	[26]
L_0	Initial SEI film thickness	0.001	Assumed
U_{SEI}	SEI formation equilibrium potential	0.4	[12,24]
ϵ_{SEI}	Porosity of SEI film	0.05	[12,24]
c_p	Constant concentration of SEI layer	28556	[12]

Table 2.2: Estimated Model Parameters for SONY 18650 lithium-ion cell monitored at 25 °C.

Parameters	COMSOL	MATLAB
k_{SEI} m/s	$1.6434 \times 10^{-17} \pm 4.3424 \times 10^{-18}$	$1.6545 \times 10^{-17} \pm 4.6825 \times 10^{-18}$
$D_s^{eff} m^2/s$	$1.4029 \times 10^{-19} \pm 4.3755 \times 10^{-20}$	$1.4213 \times 10^{-19} \pm 4.7289 \times 10^{-20}$
$D_s m^2/s$	1.2548×10^{-17}	1.2712×10^{-17}

Table 2.3: Estimated Model Parameters for SONY 18650 lithium-ion cell monitored at 35 °C.

Parameters	COMSOL	MATLAB
k_{SEI} m/s	$9.9560 \times 10^{-17} \pm 2.7989 \times 10^{-17}$	$9.5227 \times 10^{-17} \pm 2.9625 \times 10^{-17}$
$D_s^{eff} m^2/s$	$7.2369 \times 10^{-19} \pm 2.5983 \times 10^{-19}$	$8.1678 \times 10^{-19} \pm 2.7291 \times 10^{-19}$
$D_s m^2/s$	6.4728×10^{-17}	7.3055×10^{-17}

mixed model. As shown in Figure 2.3, the overall quality of the mixed mode model predictions of the OCP data for the SONY 18650 cell demonstrates that the mixed mode model provides a satisfactory description of the OCP due to the growth of the SEI, which is valid for the entire time period that the lithium-ion cells were stored under open-circuit conditions.

The kinetic rate constant k_{SEI} and the effective diffusion coefficient D_s^{eff} extracted from the curve fitting to the experimental data points at different temperatures of 25 °C and 35 °C for the SONY 18650 cell, and the SEI parameters used in the model are listed in Tables I, II and III.

In addition, confidence intervals were obtained to provide an accuracy range for the estimated parameters. The nonlinear confidence interval is shown in Figure 2.4 by producing a contour plot of the objective function with variations in the two

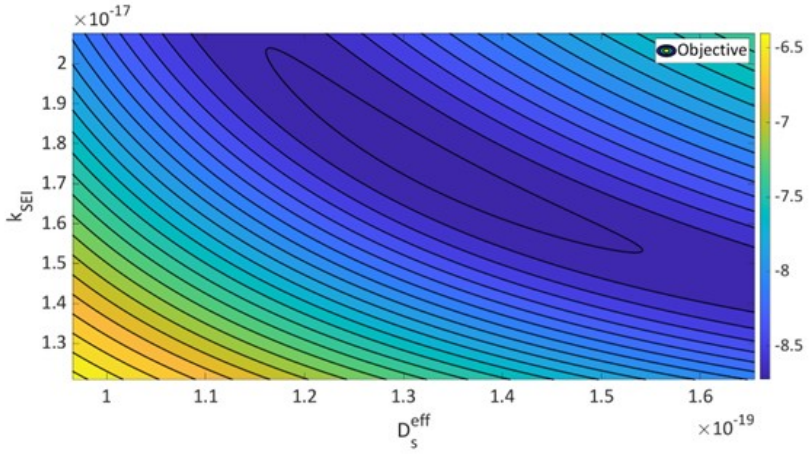

Figure 2.4: Contour plot of the objective function Obj in (2.13) as a function of kinetic rate constant and the effective diffusion coefficient

parameters. The optimal solution is shown at the center of the plot and the objective function becomes worse (higher) away from the optimal solution. As the values in Table II and III indicate, the kinetics and diffusion parameters based on the two numerical approaches (finite element and finite difference methods) are reasonably close to each other, demonstrating the credibility of the mixed mode model to simulate the growth of the SEI layer.

Solvent concentration

The current model equations have been evaluated for concentration profiles in the SEI layer for 365 days. Figure 2.5 shows the plots for the variation of concentration with time at the electrode/SEI interface of the SONY 18650 cell. Initially, solvent consumption is expected to be higher, manifested in the faster rate of SEI formation or the moving boundary velocity. Under these circumstances, the diffusion of solvent ions reaches a steady state, and the SEI layer grows faster and thicker. As the time increases, the concentration profile drops and rises as the interface shifts towards higher solvent concentrations. The drop in concentration occurs as the Li^+ ions at the interface are depleted. The rise occurs as the diffusion occurs, increasing the

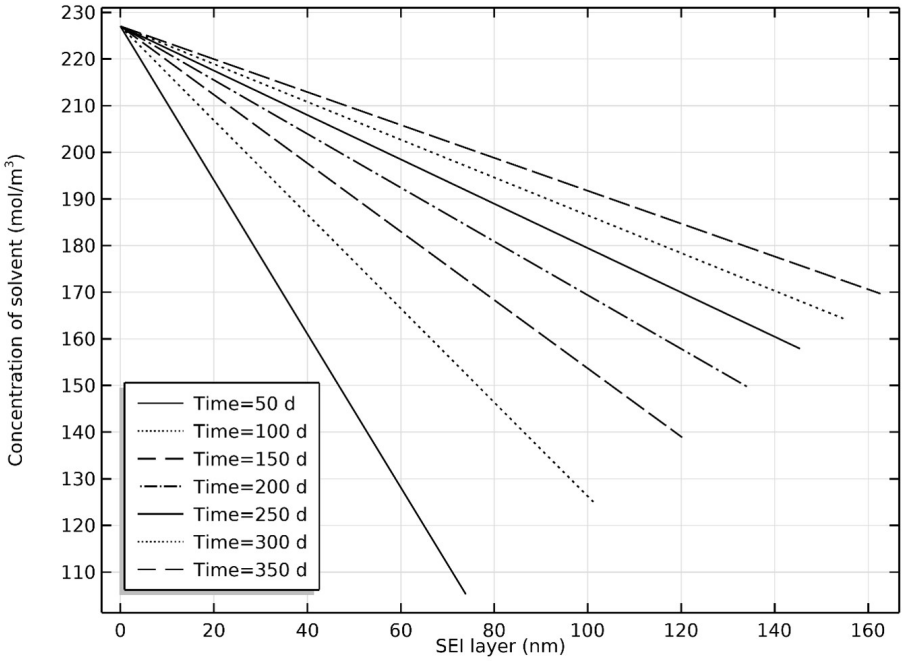

Figure 2.5: Solvent concentration versus SEI thickness in mixed mode model over 365 days.

solvent concentration at the interface as it moves.

Diffusion coefficient, kinetic rate constant and State of Charge parametric study

The chemical kinetics and transport properties of the SEI growth model, such as the kinetic rate constant of the solvent reduction reaction and diffusion coefficient of the solvent, are critical in estimating open circuit potential, SEI thickness, and capacity loss. To investigate the effect of the diffusion coefficient of the solvent, OCP predictions for different diffusion coefficient values are shown in Figure 2.6a for the SONY 18650 cell. As shown in Figure 2.6a, the higher diffusion coefficient of the solvent results in a higher OCP value due to faster diffusion of the solvent. In other words, the film growth rate at the negative electrode is greater for the higher diffusion coefficients. We did not consider the passivation effects in our model, as the long-term degradation of lithium-ion batteries is caused by the formation and continued growth

of the SEI layer.

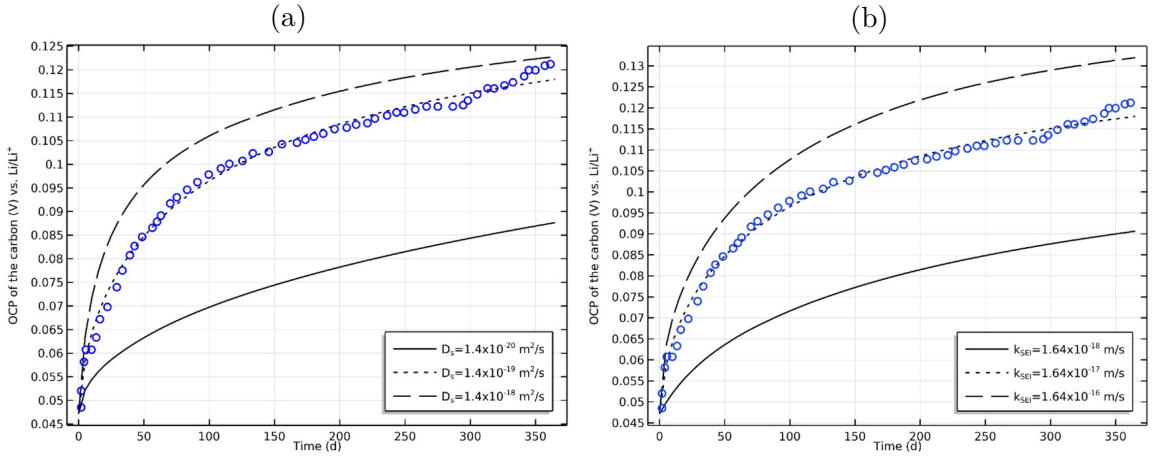

Figure 2.6: Measured (O) and simulated (-) OCP as function of time for different a) diffusion coefficient b) reaction rate constant values.

A similar parametric study was conducted to evaluate the effect of the kinetic rate constant of the solvent reduction reaction on the OCP and OCP predictions for different k_{SEI} values are shown in Figure 2.6b for the SONY 18650 cell. The solid curves fitted to the measurement data points are the simulation result for $k_{SEI} = 1.6434 \times 10^{-17}$ m/s. Figure 2.6b illustrates, OCP value increases more rapidly with time for higher value due to a higher rate of SEI formation. The dependency of the OCP on the kinetic rate constant of the solvent reduction reaction can be explained through the correlation between the Tafel kinetics and the growth rate of the SEI layer shown in Eqs. 2 and 9.

In order to investigate the effect of the SOC of the electrode, SEI thickness and capacity loss predictions for different initial SoCs are shown in Figures 7a and 7b for a SONY 18650 cell. As shown in Figure 7b, the higher SoC of the electrode results in more capacity loss. In other words, the SEI growth rate at the negative electrode is more significant for the fully charged cells than for the cells with a lower SoC, as presented in Figure 7a. In addition, at higher SoC, the OCP of the negative electrode is more cathodic to the solvent reduction potential than that of the electrode

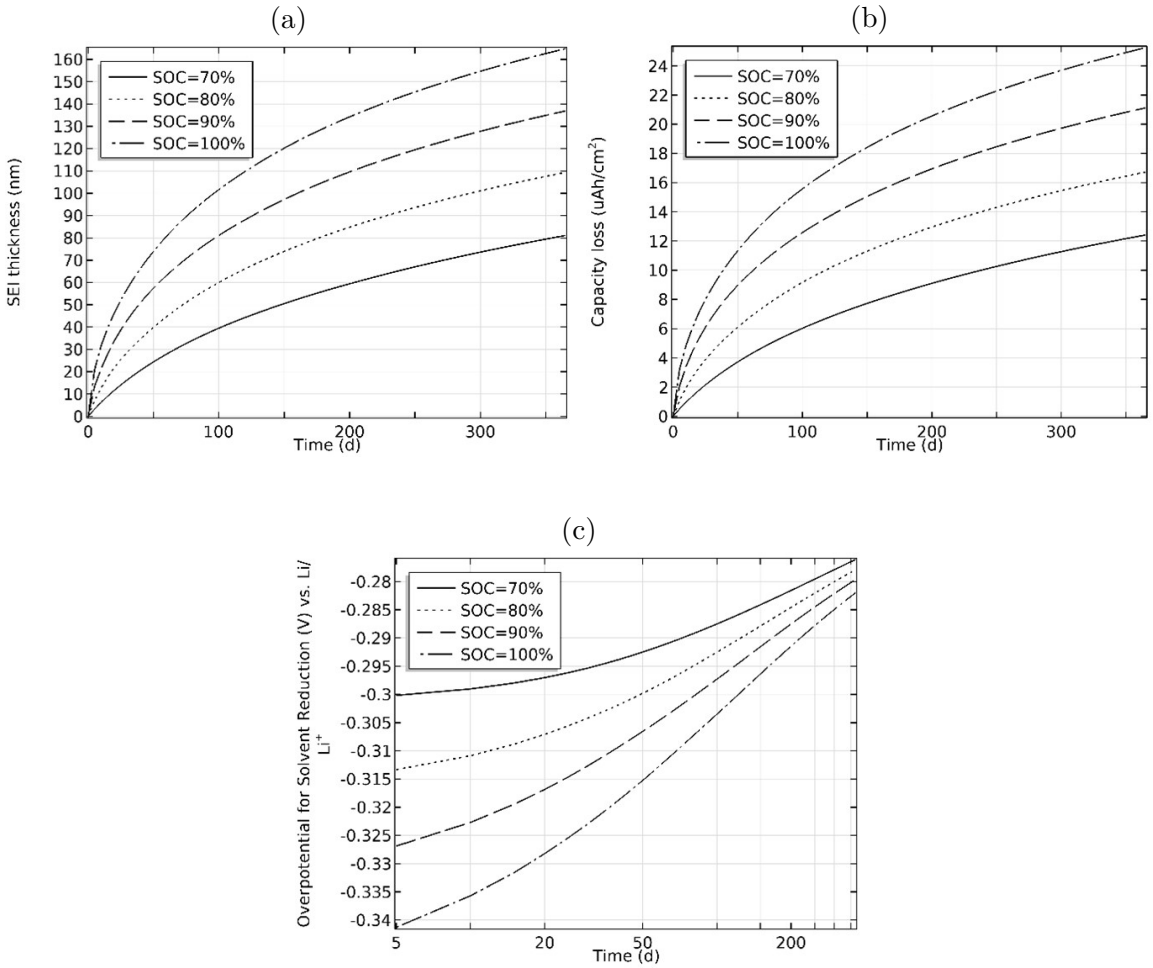

Figure 2.7: Plots of (a) SEI thickness as a function of time, (b) capacity loss due to self-discharge of the carbon electrode and (c) overpotential for solvent reduction as a function of storage time, simulated for different initial SoC values.

with lower SoC. In other words, the overpotential for the solvent reduction reaction increases with the SoC of the negative electrode, as presented in Figure 7c.

SEI thickness

It is important to understand the relationship among diffusivity, side reaction rate, and SEI layer growth characteristics. When the diffusion coefficient is small, the system becomes diffusion limited. Figure 8a shows the SEI layer growth with different diffusion coefficients for the solvent in the SEI layer. On the other hand, with a large

diffusion coefficient, the system becomes more kinetics limited. For example, with the diffusion coefficients varied by two orders of magnitude, the SEI layer grows two times thick. This is because the solvent diffuses through the porous SEI layer more easily to reach the electrode surface with a higher diffusion coefficient. Therefore, the SEI layer grows faster and thicker.

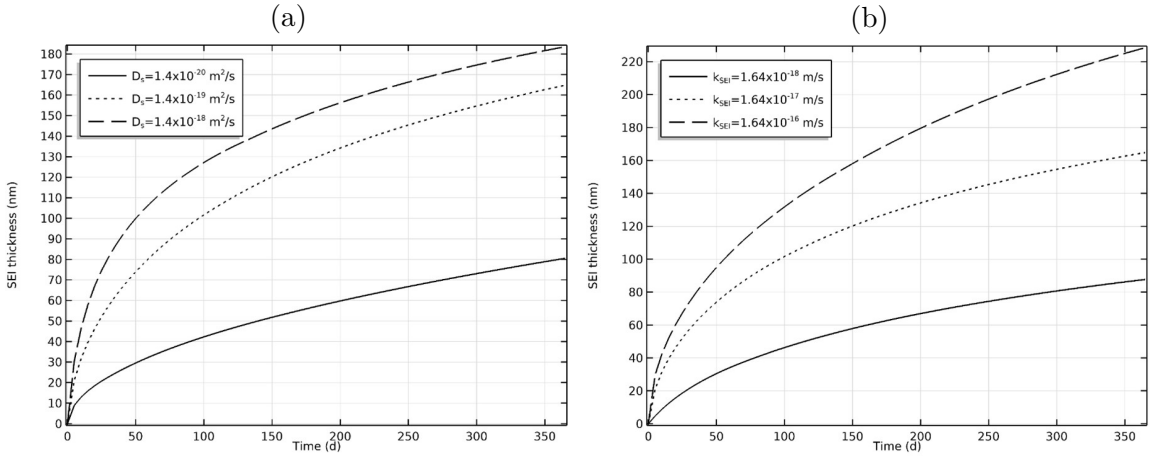

Figure 2.8: Effect of a) solvent diffusion coefficient and b) kinetic reaction rate constant on SEI growth.

The SEI layer growth also depends on the kinetics of the side reaction. Figure 8b shows the effect of the side reaction rate constant on SEI growth. The reaction rate is varied by two orders of magnitude. The SEI layer grows faster and thicker with a faster reaction rate. The overall trend is that the SEI layer grows quickly initially. This is because the initial growth of SEI is diffusion limited. Then, the growth rate gradually slows down due to the rising resistance from the layer thickness, making the system shift toward kinetic limited.

Ramasamy et al. [25] derived their expression for the SEI thickness using a kinetic limited model that increases continuously over time due to the solvent reduction reaction (see Eq. 13 in Ref. 24). In addition, they assumed the solvent is present in excess at the electrode/SEI film interface and thus do not limit the reduction reaction rate and the rate constant for the side reaction, k_{SEI} m/s to be 1.5×10^{-18}

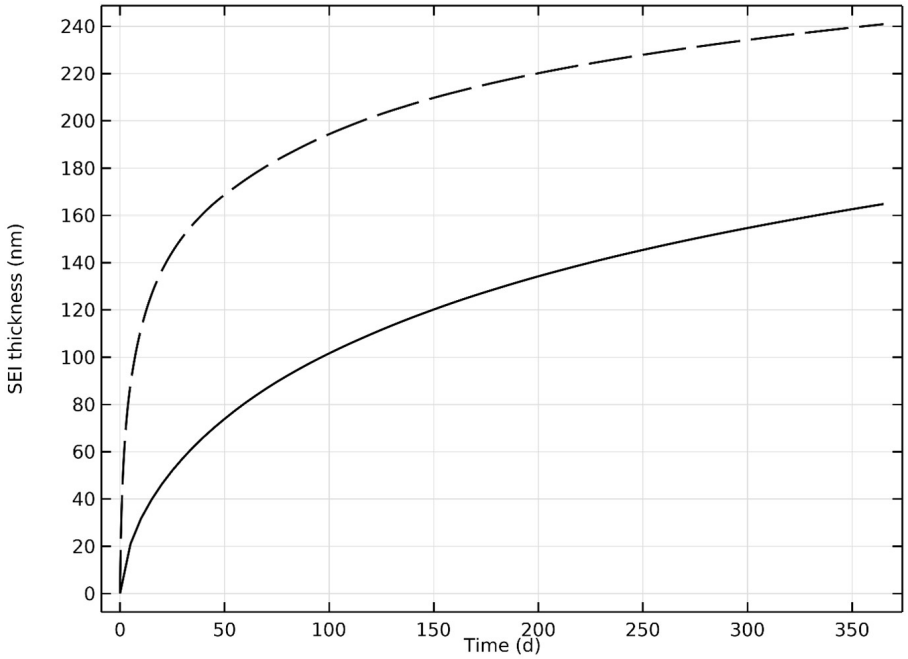

Figure 2.9: SEI thickness as a function of time in our mixed mode model (-) and reproduced solutions from reference Ramasamy et al. [24] (- -). Ramasamy et al.s Eq.13 with the rate constant of greatly deviates from our model.

(see Figure 3 caption in Ref. 24). Figure 2.9 shows their model prediction for the SEI thickness, which greatly deviates (almost 1.5 times more) from our mixed mode model prediction.

Capacity loss

The capacity loss is proportional to the current density of the side reaction. Therefore, the loss of active lithium-ions per unit surface area during storage was estimated using the following equation:

$$Capacityloss = \int_0^{t_{final}} |J_{SEI}| dt \tag{2.14}$$

Figure 2.10 shows the capacity loss due to SEI growth from our mixed-mode model and comparison with Ramasamy et al.[25] kinetic limited model that increases continuously over time due to the solvent reduction reaction (see Eq. 10 in Ref. 24).

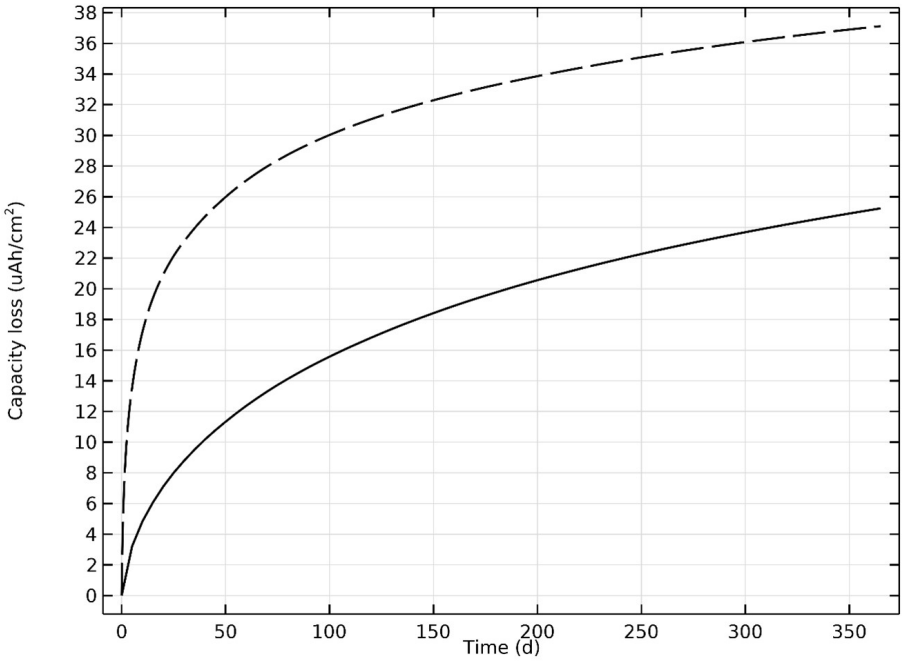

Figure 2.10: Capacity loss as a function of time in our mixed mode model (-) and reproduced solutions from reference Ramasamy et al. [24] (- -). Ramasamy et al.s Eq.10 with the rate constant of greatly deviates from our model.

Their model prediction for the capacity loss greatly deviates (almost 1.5 times more).

2.4 Conclusions

In this study, the SEI layer growth was modeled as a side reaction of solvent reduction at the anode under open-circuit conditions. The SEI grows depending on the diffusion of solvent through SEI layer and its corresponding reaction kinetics with the deintercalated lithium ions where it is associated with current density of side reaction at the electrode/SEI interface. The experimental data for OCV storage from the literature is fitted and results present the mixed mode simulation displaying lower capacity loss and thinner SEI due to its growth under open circuit condition than previous results presented by others [25]. In the OCV storage process, lithium ions will de-intercalate from the negative electrode, then the SOC reduction induces the rise of OCV value of the negative electrode. The different magnitudes of effective

diffusion coefficient of solvent and side reaction rate both play key roles in affecting SEI growth. An alternative approach, for solving partial differential equations, which fixes moving boundary problem, is computed using COMSOL and MATLAB to get parameter estimates and confidence intervals. The estimated parameters using in this work are validated with the experimental data in literature.

Chapter 3

Higher corrections of the Ilkovich equation

3.1 Introduction

The Ilkovich equation quantifies the limiting diffusion current at a dropping mercury electrode, an experimental apparatus first deployed for electrochemical measurements by Heyrovsky [49]. Ilkovich originally developed a formula for the current in the limit where the diffusion boundary layer is negligibly small compared to the mercury drop's radius. He showed that the total current flow, averaged over the droplet lifetime, is proportional to the sixth root of time [50, 51]. The model was formulated as a convective-diffusion problem by MacGillavry and Rideal [52]. A first-order correction, with an additional term up to the cube root of time, was developed by Koutecky [53], although Levich noted that the reported formula was incorrect [54]. An accurate calculation of the first-order term was presented by Newman in this journal [55]. More recently, Samec gave a compelling history of the Ilkovich problem, although it omits the later corrections of Koutecky's results by Levich and Newman [56].

The purpose of this section is to develop a second-order correction to the Ilkovich equation. We show that the instantaneous molar flowrate $N(t)$ of a solute with bulk concentration c_∞ and diffusivity D at the surface of a dropping mercury electrode supplied at volumetric flowrate Q depends on time t as[1]

$$N\left(t\right) = K_0 c_\infty Q^{2/3} D^{1/2} t^{1/6} \left[1 + K_1 \left(\frac{D^3 t}{Q^2}\right)^{1/6} + K_2 \left(\frac{D^3 t}{Q^2}\right)^{1/3} + ...\right], \tag{3.1}$$

[1]Note that the expression in equation 3.1 is given in terms of time t after the droplet begins to fall. Ilkovich reported an equation averaged over the drop time t_d.

in which K_0, K_1, and K_2 are numerical constants given by

$$\begin{aligned} K_0 &= \left(\frac{16464}{\pi}\right)^{1/6} = 4.16771085... \\ K_1 &= \frac{16 \cdot 48^{1/6}\Gamma\left(\frac{15}{14}\right)\pi^{1/3}}{11\Gamma\left(\frac{11}{7}\right)\sqrt{7}} = 1.66060563... \\ K_2 &= \frac{162^{1/3}\pi^{2/3}}{1694}\left(\frac{480\Gamma\left(\frac{15}{14}\right)\Gamma\left(\frac{8}{7}\right)}{\Gamma\left(\frac{11}{7}\right)\Gamma\left(\frac{23}{14}\right)} - 469\right) = 0.49216295..., \end{aligned} \tag{3.2}$$

and Γ represents the gamma function. Time averaging $N(t)$ over the drop time td produces the Ilkovich formula in its standard form, discussed further in sections below.

In the course of identifying these constants we introduce an asymptotic perturbation analysis that systematically produces equation systems governing terms of higher order, clarifying the earlier Newman–Levich calculation of K_1. Finally, we test our analytical results against a numerical solution of the governing system, showing that the second-order correction substantially increases the timescale across which the asymptotic model is valid.

3.2 Problem statement and nondimensionalization

Consider a spherical droplet of mercury with time-dependent radius, which grows at constant volumetric flowrate from a volume of zero at time zero. This droplet is immersed in an incompressible liquid solution containing a solute with constant diffusivity at a dilute constant bulk concentration. Also at time zero, a voltage is applied between the mercury and the bulk solution, inducing an electrochemical surface reaction that consumes the solute. The Ilkovich problem asks: given an applied voltage large enough to make the solute concentration vanish completely and immediately at the droplet boundary, how does the total molar flowrate of solute to the surface vary with time after the voltage is applied? A solution valid at times sufficiently short is given by equation 3.1 above, which we proceed to derive now.

Since the volumetric flowrate of the mercury is constant, the droplet volume at time t is

$$\tfrac{4}{3}\pi r_0^3 = Qt, \quad \text{so that} \quad r_0(t) = \left(\frac{3Q}{4\pi}\right)^{1/3} t^{1/3}, \tag{3.3}$$

i.e., the droplet's radius r_0 grows with the cube root of time. The only nonzero component of the fluid velocity is radial, v_r, and the flow satisfies $v_r(t, r_0) = dr_0/dt$ at the droplet surface. Thus, since the dilute condition ensures that the fluid's density is constant, mass continuity requires that the flow field for all $r \geq r_0$ is

$$v_r(r) = \frac{Q}{4\pi r^2}. \tag{3.4}$$

Conveniently, the constancy of Q guarantees that this relationship is independent of time. To illustrate the solute's transient behavior, we seek a concentration distribution $c(t, r)$ that satisfies the radial spherical convective diffusion governing equation (GE)

$$\text{GE:} \quad \frac{\partial c}{\partial t} + v_r(r)\frac{\partial c}{\partial r} = D\left(\frac{2}{r}\frac{\partial c}{\partial r} + \frac{\partial^2 c}{\partial r^2}\right), \tag{3.5}$$

subject to an initial condition (IC)

$$\text{IC:} \quad c(0, r) = c_\infty, \tag{3.6}$$

as well as inner and outer boundary conditions (BCi and BCii, respectively)

$$\text{BCi:} \quad c(t, r_0(t)) = 0 \quad \text{and} \quad \text{BCii:} \quad c(t, \infty) = c_\infty. \tag{3.7}$$

Solving the system of equations 3.5-3.7 will enable computation of the excess molar flux, which is proportional to the concentration gradient at the droplet surface.

First nondimensionalize the problem to simplify the system of equations. Observe that different powers of parameters D and Q can be combined to identify characteristic length and time scales; inspection of the dimensional matrix for this system shows that it affords three dimensionless degrees of freedom. By changing variables to

$$C = \frac{c - c_\infty}{c_\infty}, \quad T = \frac{16\pi^2 D^3 t}{Q^2}, \quad \text{and} \quad R = \frac{4\pi D r}{Q}, \tag{3.8}$$

the equation system can be cast dimensionlessly as

$$\text{GE:}\quad \frac{\partial C}{\partial T}+\frac{1}{R^2}\frac{\partial C}{\partial R}=\frac{2}{R}\frac{\partial C}{\partial R}+\frac{\partial^2 C}{\partial R^2} \tag{3.9}$$

$$\text{IC:}\quad C\left(0,R\right)=0 \tag{3.10}$$

$$\text{BCi:}\quad C\left(T,\left(3T\right)^{1/3}\right)=-1 \qquad \text{BCii:}\quad C\left(T,\infty\right)=0. \tag{3.11}$$

Here we see why the Ilkovich problem is particularly interesting: it yields a model of the system response with no free parameters. Hence it should be possible to establish a universal solution applicable to many different experimental situations.

Analytical approaches to solve equations 3.9-3.11 are impeded by the fact that BCi sits on a moving boundary, a difficulty resolved by changing coordinates. The moving boundary can be made stationary by introducing a new position descriptor that puts the radial coordinate in units of the droplet radius. Also, since the concentration distribution close to the droplet is of primary interest, it is prudent to translate this position such that BCi moves to the origin. To establish new coordinates take

$$\mathrm{t}\left(T,R\right)=T \quad \text{and} \quad \mathrm{r}\left(T,R\right)=\frac{R}{\left(3T\right)^{1/3}}-1. \tag{3.12}$$

The Jacobian of this coordinate transformation is

$$\begin{aligned} \frac{\partial \mathrm{t}}{\partial T}&=1 & \frac{\partial \mathrm{t}}{\partial R}&=0,\\ \frac{\partial \mathrm{r}}{\partial T}&=-\frac{R}{\left(3T\right)^{4/3}}=-\frac{\mathrm{r}+1}{3\mathrm{t}} & \frac{\partial \mathrm{r}}{\partial R}&=\frac{1}{\left(3T\right)^{1/3}}=\frac{1}{\left(3\mathrm{t}\right)^{1/3}}. \end{aligned} \tag{3.13}$$

Thus, according to the chain rule, the derivatives of C in the original laboratory frame $\{T,R\}$ and the new coordinates $\{\mathrm{t},\mathrm{r}\}$, in which the inner boundary is fixed to the droplet surface and the radial coordinate is normalized by the droplet radius relate, through

$$\begin{aligned} \frac{\partial C}{\partial T}&=\frac{\partial C}{\partial \mathrm{t}}\frac{\partial \mathrm{t}}{\partial T}+\frac{\partial C}{\partial \mathrm{r}}\frac{\partial \mathrm{r}}{\partial T}=\frac{\partial C}{\partial \mathrm{t}}-\frac{(\mathrm{r}+1)}{3\mathrm{t}}\frac{\partial C}{\partial \mathrm{r}},\\ \frac{\partial C}{\partial R}&=\frac{\partial C}{\partial \mathrm{t}}\frac{\partial \mathrm{t}}{\partial R}+\frac{\partial C}{\partial \mathrm{r}}\frac{\partial \mathrm{r}}{\partial R}=\frac{1}{\left(3\mathrm{t}\right)^{1/3}}\frac{\partial C}{\partial \mathrm{r}}, \qquad \text{and}\\ \frac{\partial^2 C}{\partial R^2}&=\left[\frac{\partial}{\partial \mathrm{t}}\left(\frac{\partial C}{\partial R}\right)\right]\frac{\partial \mathrm{t}}{\partial R}+\left[\frac{\partial}{\partial \mathrm{r}}\left(\frac{\partial C}{\partial R}\right)\right]\frac{\partial \mathrm{r}}{\partial R}=\frac{1}{\left(3\mathrm{t}\right)^{2/3}}\frac{\partial^2 C}{\partial \mathrm{r}^2}. \end{aligned} \tag{3.14}$$

Incorporation of relations 3.12 and 3.14 transforms the Ilkovich problem to

$$\text{GE:}\quad \frac{\partial C}{\partial \mathrm{t}} + \frac{1}{3\mathrm{t}}\left[\frac{1}{(1+\mathrm{r})^2} - 1 - \mathrm{r}\right]\frac{\partial C}{\partial \mathrm{r}} = \frac{1}{(3\mathrm{t})^{2/3}}\left(\frac{2}{1+\mathrm{r}}\frac{\partial C}{\partial \mathrm{r}} + \frac{\partial^2 C}{\partial \mathrm{r}^2}\right) \tag{3.15}$$

$$\text{IC:}\quad C(0,\mathrm{r}) = 0 \tag{3.16}$$

$$\text{BCi:}\quad C(\mathrm{t},0) = -1 \qquad \text{BCii:}\quad C(\mathrm{t},\infty) = 0. \tag{3.17}$$

The new independent variables simplify BCi and BCii at the expense of complicating GE. Nevertheless, the formulation should be readily tractable numerically and is a useful starting point for asymptotics.

3.3 Asymptotic analysis and regular perturbation

Since the Ilkovich problem is phrased over a semi-infinite spatial domain, one might expect the system of equations 3.15-3.17 to be amenable to a similarity transformation. Because it affords three dimensionless degrees of freedom, however, this system is not a self-similar problem of the first kind. The key difficulty is that the convective part of the response (described by the left side of equation 3.15) scales differently with time than the diffusional part (the right side of equation 3.15). One typically expects diffusion boundary layers to grow with the square root of time, but the simultaneous growth of the droplet radius confounds this intuition.

Some practical considerations help to guide the next steps. In a typical experimental apparatus for falling-drop experiments, mercury droplets grow to a maximum diameter of approximately 0.1 cm. A reasonable estimate of the drop time—the time taken for the droplet to grow to its maximum size before falling off the capillary tube that supplies it—is $t_\mathrm{d} = 10s$. The fastest diffusivities that solutes exhibit in water are around $5 \cdot 10^{-5} cm^2 s^{-1}$. Taking all of this into account, the maximum time that concerns us is a dimensionless drop time, $\mathrm{t_d}$, of order

$$\mathrm{t_d} = \frac{16\pi^2 D^3 t_\mathrm{d}}{Q^2} \approx 10^{-1}. \tag{3.18}$$

Thus analysis of system 3.15-3.17 can be limited to small times. We assume that $\mathrm{t} << 1$ moving forward.

One also expects that the concentration distribution varies transiently within a diffusion boundary layer, whose penetration depth should grow with time. Therefore renormalize coordinates again, to amplify the scale of radial positions near the boundary at small times:

$$\mathrm{T}\left(\mathrm{t},\mathrm{r}\right)=\mathrm{t} \quad \text{and} \quad \eta\left(\mathrm{t},\mathrm{r}\right)=\frac{\mathrm{r}}{\mathrm{t}^{\alpha}}. \tag{3.19}$$

For this transformation, the Jacobian is

$$\begin{aligned} \frac{\partial \mathrm{T}}{\partial \mathrm{t}} &= 1 & \frac{\partial \mathrm{T}}{\partial \mathrm{r}} &= 0, \\ \frac{\partial \eta}{\partial \mathrm{t}} &= -\frac{\alpha \mathrm{r}}{\mathrm{t}^{\alpha+1}} = -\frac{\alpha\eta}{\mathrm{T}} & \frac{\partial \eta}{\partial \mathrm{r}} &= \frac{1}{\mathrm{t}^{\alpha}} = \frac{1}{\mathrm{T}^{\alpha}}. \end{aligned} \tag{3.20}$$

In terms time T and the similarity variable η, the concentration derivatives with respect to t and r become

$$\begin{aligned} \frac{\partial C}{\partial \mathrm{t}} &= \frac{\partial C}{\partial \mathrm{T}}\frac{\partial \mathrm{T}}{\partial \mathrm{t}} + \frac{\partial C}{\partial \eta}\frac{\partial \eta}{\partial \mathrm{t}} = \frac{\partial C}{\partial \mathrm{T}} - \frac{\alpha\eta}{\mathrm{T}}\frac{\partial C}{\partial \eta}, \\ \frac{\partial C}{\partial \mathrm{r}} &= \frac{\partial C}{\partial \mathrm{T}}\frac{\partial \mathrm{T}}{\partial \mathrm{r}} + \frac{\partial C}{\partial \eta}\frac{\partial \eta}{\partial \mathrm{r}} = \frac{1}{\mathrm{T}^{\alpha}}\frac{\partial C}{\partial \eta}, \qquad \text{and} \\ \frac{\partial^2 C}{\partial \mathrm{r}^2} &= \left[\frac{\partial}{\partial \mathrm{T}}\left(\frac{\partial C}{\partial \mathrm{r}}\right)\right]\frac{\partial \mathrm{T}}{\partial r} + \left[\frac{\partial}{\partial \eta}\left(\frac{\partial C}{\partial \mathrm{r}}\right)\right]\frac{\partial \eta}{\partial \mathrm{r}} = \frac{1}{\mathrm{T}^{2\alpha}}\frac{\partial^2 C}{\partial \eta^2} \end{aligned} \tag{3.21}$$

via the chain rule. With the relationships from equations 3.19 and 3.21, the governing system transforms to

$$\text{GE:}\quad \frac{\partial C}{\partial \mathrm{T}} + \frac{1}{3\mathrm{T}^{\alpha+1}}\left[\frac{1}{\left(1+\eta\mathrm{T}^{\alpha}\right)^2} - 1 - \left(3\alpha+1\right)\eta\mathrm{T}^{\alpha}\right]\frac{\partial C}{\partial \eta} = \frac{1}{3^{2/3}\mathrm{T}^{2/3+2\alpha}}\left(\frac{\partial^2 C}{\partial \eta^2} + \frac{2\mathrm{T}^{\alpha}}{1+\eta\mathrm{T}^{\alpha}}\frac{\partial C}{\partial \eta}\right) \tag{3.22}$$

$$\text{IC:}\quad \lim_{\eta\to\infty} C\left(0,\eta\right) = 0 \tag{3.23}$$

$$\text{BCi:}\quad C\left(\mathrm{T},0\right) = -1 \qquad \text{BCii:}\quad C\left(\mathrm{T},\infty\right) = 0. \tag{3.24}$$

As mentioned before, one does not expect $\alpha = 1/2$ because of the radial convection. Instead some other positive power of time will balance the scale of the convective term on the left of GE 3.3 with that of the diffusional term on the right.

To perform the balancing of GE 3.3, exploit the conclusion illustrated by equation 3.18, that the dimensionless time is small. Since $\mathrm{T}(\mathrm{t},\mathrm{r}) = \mathrm{t}$, $\mathrm{T} << 1$ if t is, and consequently one can replace the following functions of $\eta\mathrm{T}^\alpha$ with their Maclaurin expansions:

$$\frac{1}{1+\eta\mathrm{T}^\alpha} = \sum_{k=0}^{\infty}(-1)^k(\eta\mathrm{T}^\alpha)^k \quad \text{and} \quad \frac{1}{(1+\eta\mathrm{T}^\alpha)^2} = \sum_{k=0}^{\infty}(k+1)(-1)^k(\eta\mathrm{T}^\alpha)^k. \quad (3.25)$$

Thus GE 3.3 can be rewritten for small T when $\eta = O(1)$ as

$$\text{GE:}\ \frac{\partial C}{\partial \mathrm{T}} - \frac{\eta}{\mathrm{T}}\left[1+\alpha-\eta\mathrm{T}^\alpha\sum_{k=0}^{\infty}\left(1+\tfrac{1}{3}k\right)(-1)^k(\eta\mathrm{T}^\alpha)^k\right]\frac{\partial C}{\partial \eta} = \frac{1}{3^{2/3}\mathrm{T}^{2/3+2\alpha}}\left[\frac{\partial^2 C}{\partial \eta^2} + 2\mathrm{T}^\alpha\frac{\partial C}{\partial \eta}\sum_{k=1}^{\infty}(-1)^k(\eta\mathrm{T}^\alpha)^k\right]. \quad (3.26)$$

In the limit of small T, the sums in equation 3.77 are negligible compared to the other terms in the square brackets containing them. To ensure that diffusion and convection within the boundary layer are of equal importance in the small-T limit, choose α to balance the exponent of T in the steady convective terms on the left with the exponent on the leading diffusional term on the right. That is, take

$$1 = \frac{2}{3} + 2\alpha \quad \Longrightarrow \quad \alpha = \frac{1}{6}. \quad (3.27)$$

After choosing $\alpha = 1/6$, the Ilkovich problem becomes

$$\text{GE:}\ \frac{1}{3^{2/3}}\frac{\partial^2 C}{\partial \eta^2} + \frac{7}{6}\eta\frac{\partial C}{\partial \eta} = \mathrm{T}\frac{\partial C}{\partial \mathrm{T}} + \mathrm{T}^{1/6}\frac{\partial C}{\partial \eta}\sum_{k=0}^{\infty}\left[\left(1+\frac{k}{3}\right)\eta^2 - \frac{2}{3^{2/3}}\right](-\eta)^k\,\mathrm{T}^{k/6} \quad (3.28)$$

$$\text{IC:}\ \lim_{\eta\to\infty} C(0,\eta) = 0 \quad (3.29)$$

$$\text{BCi:}\ C(\mathrm{T},0) = -1 \qquad \text{BCii:}\ C(\mathrm{T},\infty) = 0. \quad (3.30)$$

The left side of GE 3.28 relates to the standard Cartesian diffusion-layer penetration problem, whose solution can be used to derive Ilkovich's original equation.

To simplify notation and introduce a new time scaling that will help in subsequent analysis, it is convenient to rescale the position variable such that the left side of equation 3.28 becomes the error-function differential equation, as well as introducing a new time variable proportional to $\mathrm{T}^{1/6}$ that makes the right side of GE 3.28 depend on integer powers of time. The choices

$$\tau\left(\mathrm{T},\eta\right)=\frac{2}{\sqrt{7}}\left(3\mathrm{T}\right)^{1/6}\quad\text{ and }\quad\xi\left(\mathrm{T},\eta\right)=\frac{\eta\sqrt{7}}{2\cdot3^{1/6}} \tag{3.31}$$

simplify the governing system to

$$\text{GE: }\ \frac{\partial^2 C}{\partial\xi^2}+2\xi\frac{\partial C}{\partial\xi}=\frac{2\tau}{7}\frac{\partial C}{\partial\tau}+2\tau\frac{\partial C}{\partial\xi}\sum_{k=0}^{\infty}\left(-1\right)^k\left[\frac{6}{7}\left(1+\frac{k}{3}\right)\xi^2-1\right]\xi^k\tau^k \tag{3.32}$$

$$\text{IC: }\ \lim_{\xi\to\infty}C\left(0,\xi\right)=0 \tag{3.33}$$

$$\text{BCi: }\ C\left(\tau,0\right)=-1\qquad\text{BCii: }\ C\left(\tau,\infty\right)=0. \tag{3.34}$$

This restatement clarifies that all the terms on the right are of order τ or higher. By neglecting these terms, one obtains the problem Ilkovich originally solved.

Observe that the transformed independent variables τ and ξ relate to the original, dimensional quantities r and t through

$$\tau\left(r,t\right)=\frac{2}{\sqrt{7}}\left(\frac{48\pi^2D^3t}{Q^2}\right)^{1/6}\quad\text{ and }\quad\xi\left(r,t\right)=\left[r-r_0\left(t\right)\right]\sqrt{\frac{7}{12Dt}}, \tag{3.35}$$

where $r_0\left(t\right)$ is defined in equation 3.3. These differ slightly from transformations used in the past, although they relate in a straightforward way. For example, Newman used a time variable that can be identified as $\left(\tau/2\right)^{14}$, and a similarity variable equal to $2\xi\left(\tau/2\right)^7$ [55].

Corrections to the Ilkovich equation can be obtained by perturbation expansion of the system of equations 3.32-3.34 with respect to time. To implement this assume that concentration has the form

$$C\left(\tau,\xi\right)=C_0\left(\xi\right)+\tau C_1\left(\xi\right)+\tau^2C_2\left(\xi\right)+... \tag{3.36}$$

and equate terms with similar powers of τ to formulate a sequence systems that govern approximations to C of increasing order. Observe that at every order, IC

and BCii from equations 3.33 and 3.34 collapse to a single condition at $\xi \to \infty$. At noughth order, one finds that

$$\mathrm{GE}_0\text{:}\quad \frac{d^2C_0}{d\xi^2} + 2\xi\frac{dC_0}{d\xi} = 0 \tag{3.37}$$

$$\mathrm{BCi}_0\text{:}\quad C_0\left(0\right) = -1 \qquad \mathrm{BCii}_0\text{:}\quad C_0\left(\infty\right) = 0; \tag{3.38}$$

at integer orders $n \geq 1$ one finds

$$\mathrm{GE}_n\text{:}\quad \frac{d^2C_n}{d\xi^2} + 2\xi\frac{dC_n}{d\xi} - \frac{2n}{7}C_n = 2\sum_{k=1}^{n}\left(-1\right)^k\left[1 - \tfrac{2}{7}\left(2+k\right)\xi^2\right]\xi^{k-1}\frac{dC_{n-k}}{d\xi} \tag{3.39}$$

$$\mathrm{BCi}_n\text{:}\quad C_n\left(0\right) = 0 \qquad \mathrm{BCii}_n\text{:}\quad C_n\left(\infty\right) = 0. \tag{3.40}$$

Every positive order of the problem presents an inhomogeneous, linear second-order ordinary differential equation involving the operator that appears in the error-function differential equation (albeit of negative fractional degree). This sequence provides the systematic route by which higher-order corrections to the Ilkovich equation can be calculated.

3.4 Solution

The noughth-order problem (equations 3.37 and 3.38) is solved by

$$C_0\left(\xi\right) = -\mathrm{erfc}\left(\xi\right), \tag{3.41}$$

which is plotted in figure 3.1. Bear in mind that

$$\frac{dC_0}{d\xi} = \frac{2e^{-\xi^2}}{\sqrt{\pi}}, \tag{3.42}$$

which is needed to write the first-order problem. At first order

$$\mathrm{GE}_1\text{:}\quad \frac{d^2C_1}{d\xi^2} + 2\xi\frac{dC_1}{d\xi} - \frac{2}{7}C_1 = \frac{4}{\sqrt{\pi}}\left(\frac{6\xi^2}{7} - 1\right)e^{-\xi^2} \tag{3.43}$$

$$\mathrm{BCi}_1\text{:}\quad C_1\left(0\right) = 0 \qquad \mathrm{BCii}_1\text{:}\quad C_1\left(\infty\right) = 0. \tag{3.44}$$

Simplify by letting

$$C_1\left(\xi\right) = e^{-\xi^2}f_1\left(\xi\right), \tag{3.45}$$

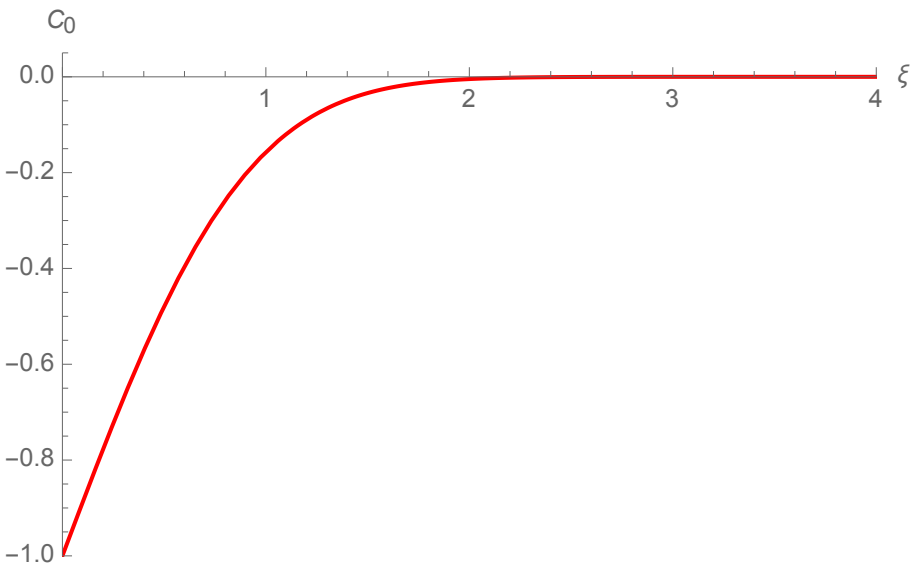

Figure 3.1: Solution for the concentration distribution C_0 from equation 3.41, which satisfies the zero-order Ilkovich model, equations 3.37 and 3.38.

in which case GE_1 from equation 3.43 becomes

$$\mathrm{GE}_{1'}\text{:}\quad \frac{d^2 f_1}{d\xi^2} - 2\xi\frac{df_1}{d\xi} - \frac{16}{7}f_1 = \frac{4}{\sqrt{\pi}}\left(\frac{6\xi^2}{7} - 1\right). \tag{3.46}$$

The solution to this can be broken up as $f_1 = f_1^{\mathrm{h}} + f_1^{\mathrm{p}}$. To identify a particular solution, guess that it takes the form of a second-order polynomial,

$$f_1^{\mathrm{p}}(\xi) = X'\xi^2 + Y'\xi + Z', \tag{3.47}$$

in which X', Y', and Z' are unknown constants. Substituting equation 3.47 into equation 3.46 and balancing its coefficients with those of the inhomogeneous polynomial in equation 3.46 yields

$$\frac{2}{7}\left(7X' - 8Z' + \frac{14}{\sqrt{\pi}}\right) - \frac{30Y'}{7}\xi + \frac{2}{7}\left(-22X' - \frac{12}{\sqrt{\pi}}\right)\xi^2 = 0 \tag{3.48}$$

Linear independence of the terms in this expression requires that the coefficients of each power of ξ vanish. The values of X', Y', and Z' that satisfy this criterion show that

$$f_1^{\mathrm{p}}(\xi) = \frac{14}{11\sqrt{\pi}} - \frac{6\xi^2}{11\sqrt{\pi}} \tag{3.49}$$

is a particular solution of $\mathrm{GE}_{1'}$. The remaining homogeneous problem satisfied by $f_1^{\mathrm{h}}(\xi)$,

$$\mathrm{GE}_{1''}\text{:}\quad \frac{d^2 f_1^{\mathrm{h}}}{d\xi^2} - 2\xi \frac{df_1^{\mathrm{h}}}{d\xi} - \frac{16}{7} f_1^{\mathrm{h}} = 0 \tag{3.50}$$

is recognized as the (physicist's) Hermite differential equation, of order $-8/7$. A closed-form solution in terms of two linearly independent functions is given on page 1353 of Weisstein's book [57]:

$$f_1^{\mathrm{h}}(\xi) = W' M(\tfrac{4}{7}, \tfrac{1}{2}, \xi^2) + V' H_{-8/7}(\xi). \tag{3.51}$$

Here $M(a, b, \xi)$ is Kummer's confluent hypergeometric function of the first kind and $H_\lambda(\xi)$ is the Hermite polynomial of order λ.[2] Because $M(a, b, \xi)$ diverges faster than $\exp(\xi^2)$ as ξ approaches infinity, condition BCii_1 requires that $W' = 0$. Condition BCi_1 then requires that $f_1^{\mathrm{h}}(0) = -f_1^{\mathrm{p}}(0)$, leaving

$$V' H_{-8/7}(0) = -\frac{14}{11\sqrt{\pi}}, \tag{3.52}$$

so that

$$V' = -\frac{28 \cdot 2^{1/7} \Gamma\left(\frac{15}{14}\right)}{11\pi}. \tag{3.53}$$

Thus the choice of particular solution demands that the homogeneous solution takes the form

$$f_1^{\mathrm{h}}(\xi) = -\frac{28 \cdot 2^{1/7} \Gamma\left(\frac{15}{14}\right)}{11\pi} H_{-8/7}(\xi). \tag{3.54}$$

[2]Hermite polynomials are continued over orders that are not whole numbers through the definition

$$H_\lambda(z) = 2^\lambda \sqrt{\pi} \left[\frac{M\left(-\frac{\lambda}{2}, \frac{1}{2}, z^2\right)}{\Gamma\left(\frac{1-\lambda}{2}\right)} - \frac{2z M\left(\frac{1-\lambda}{2}, \frac{3}{2}, z^2\right)}{\Gamma\left(-\frac{\lambda}{2}\right)} \right].$$

where $M(a, b, z)$ is Kummer's confluent hypergeometric function of the first kind. In general

$$\frac{d}{dz} H_\lambda(z) = 2\lambda H_{\lambda-1}(z)$$

and $H_\lambda(0) = 2^\lambda \sqrt{\pi} / \Gamma\left(\frac{1}{2} - \frac{1}{2}\lambda\right)$.

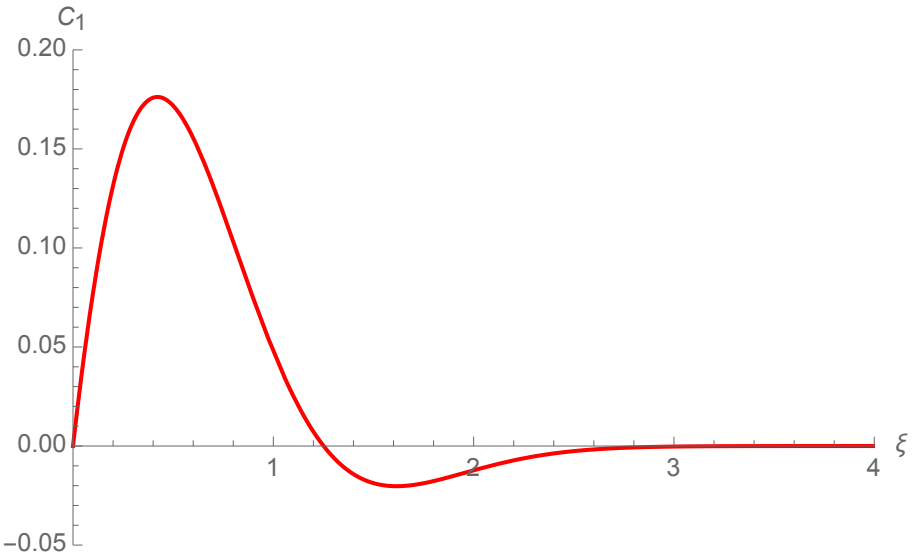

Figure 3.2: Solution for the concentration distribution C_1 from equation 3.55, which satisfies the first-order correction of the Ilkovich model, equations 3.43 and 3.44. Note the difference in vertical scale from Figure 3.1.

Adding the functions f_1^{h} and f_1^{p} from equations 3.54 and 3.49 together to form f_1 in equation 3.45, the first-order correction of the solute concentration is found to be

$$C_1(\xi) = \frac{2e^{-\xi^2}}{11\sqrt{\pi}}\left[7 - 3\xi^2 - \frac{7\cdot 2^{8/7}\Gamma\left(\frac{15}{14}\right)}{\sqrt{\pi}} H_{-8/7}(\xi)\right], \tag{3.55}$$

which is depicted in figure 3.2. The first derivative of this function at the boundary is

$$\left.\frac{dC_1}{d\xi}\right|_{\xi=0} = \frac{16\Gamma\left(\frac{15}{14}\right)}{11\Gamma\left(\frac{11}{7}\right)\sqrt{\pi}} \approx 0.88780399..., \tag{3.56}$$

a form very similar to Newman's equation 25 [55].

Solving the second-order problem is more of a grind, but an essentially similar approach can be taken. Equation 3.39 shows that

$$\mathrm{GE}_2\text{:}\quad \frac{d^2C_2}{d\xi^2} + 2\xi\frac{dC_2}{d\xi} - \frac{4}{7}C_2 = 2\left(1 - \tfrac{8}{7}\xi^2\right)\xi\frac{dC_0}{d\xi} - 2\left(1 - \tfrac{6}{7}\xi^2\right)\frac{dC_1}{d\xi}. \tag{3.57}$$

Apply the transformation in equation 3.45 to C_2 and C_1, then insert equation 3.42 to show that

$$\mathrm{GE}_{2'}\text{:}\quad \frac{d^2f_2}{d\xi^2} - 2\xi\frac{df_2}{d\xi} - \frac{18}{7}f_2 = -\frac{4}{\sqrt{\pi}}\left(1 - \tfrac{8}{7}\xi^2\right)\xi - 2\left(1 - \tfrac{6}{7}\xi^2\right)\left(\frac{df_1}{d\xi} - 2\xi f_1\right). \tag{3.58}$$

Equations 3.49 and 3.54 combine to establish the function $f_1(\xi)$ that appears here:

$$f_1(\xi) = \frac{14}{11\sqrt{\pi}} - \frac{6\xi^2}{11\sqrt{\pi}} - \frac{28 \cdot 2^{1/7}\Gamma\left(\frac{15}{14}\right)}{11\pi} H_{-8/7}(\xi). \tag{3.59}$$

After substitution of $f_1(\xi)$, the right side of equation 3.58 is observed to comprise two parts, one of which is a simple polynomial of ξ; because $dH_\lambda/d\xi = 2\lambda H_{\lambda-1}$, the other part is a linear combination of $H_{-8/7}(\xi)$ and $H_{-15/7}(\xi)$, with coefficients that are polynomials of ξ. Exploiting the linearity of $\mathrm{GE}_{2'}$, the particular solution can be broken into two parts,

$$f_2^{\mathrm{p}}(\xi) = f_2^{\mathrm{p}1}(\xi) + f_2^{\mathrm{p}2}(\xi), \tag{3.60}$$

where $f_2^{\mathrm{p}1}$ accounts for the simple-polynomial dependence and $f_2^{\mathrm{p}2}$ accounts for the Hermite-polynomial dependence. Guessing an arbitrary fifth-order polynomial shows that the simple polynomial part of the inhomogeneous term in equation 3.58 is balanced by a particular solution

$$f_2^{\mathrm{p}1}(\xi) = -\frac{1}{121\sqrt{\pi}}\left(18\xi^5 - \frac{424}{3}\xi^3 + \frac{903}{8}\xi\right). \tag{3.61}$$

The inhomogeneous terms dependent on Hermite polynomials can also be balanced by the method of trial functions, although the procedure is more convoluted. Guess the form

$$f_2^{\mathrm{p}2}(\xi) = \left(A'\xi^3 + B'\xi^2 + C'\xi + D'\right) f_1^{\mathrm{h}}(\xi) + \left(E'\xi^3 + F'\xi^2 + G'\xi + H'\right)\frac{df_1^{\mathrm{h}}}{d\xi}, \tag{3.62}$$

where $f_1^{\mathrm{h}}(\xi)$ is given by equation 3.54 and A', B', ..., H' are arbitrary parameters. Observe that since f_1^{h} satisfies the homogeneous version of $\mathrm{GE}_{1'}$ from equation 3.46 (that is, Hermite's equation of order $-8/7$) by definition, higher derivatives can be eliminated in favor of first and second derivatives:

$$\frac{d^2 f_1^{\mathrm{h}}}{d\xi^2} = 2\xi\frac{df_1^{\mathrm{h}}}{d\xi} + \frac{16}{7}f_1^{\mathrm{h}} \quad \text{and} \quad \frac{d^3 f_1^{\mathrm{h}}}{d\xi^3} = \left(4\xi^2 + \frac{30}{7}\right)\frac{df_1^{\mathrm{h}}}{d\xi} + \frac{32}{7}\xi f_1^{\mathrm{h}}. \tag{3.63}$$

Thus, upon substitution of equation 3.62 into the form of equation 3.58 obtained after discarding the polynomial part of the inhomogeneous term, and after using

equations 3.63 to limit the Hermite polynomials involved to $H_{-8/7}(\xi)$ and $H_{-15/7}(\xi)$, one obtains an equation that can be balanced by choosing appropriate values of the constants A', B', ..., H'. This balancing yields

$$f_2^{\mathrm{p2}}(\xi) = \frac{\xi}{11}\left(6\xi^2 - \frac{31}{2}\right) f_1^{\mathrm{h}}(\xi) - \frac{1}{11}\left(3\xi^2 - \frac{35}{4}\right)\frac{df_1^{\mathrm{h}}}{d\xi}. \tag{3.64}$$

With both parts of the particular solution identified, the homogeneous problem can be solved. Boundary condition BCii_2 is satisfied by a solution of the form

$$f_2^{\mathrm{h}}(\xi) = K' H_{-9/7}(\xi), \tag{3.65}$$

in which the constant K' is chosen to satisfy BCi_2: $f_2^{\mathrm{h}}(0) + f_2^{\mathrm{p1}}(0) + f_2^{\mathrm{p2}}(0) = 0$. Ultimately, after returning to the original variable $C_2(\xi)$, one finds that

$$C_2(\xi) = \frac{8e^{-\xi^2}}{121\sqrt{\pi}}\left[-\frac{35\cdot 2^{2/7}\Gamma\left(\frac{15}{14}\right)\Gamma\left(\frac{8}{7}\right)}{\sqrt{\pi}\Gamma\left(\frac{11}{7}\right)}H_{-9/7}(\xi) - \frac{9}{4}\xi^5 + \frac{53}{3}\xi^3 - \frac{903}{64}\xi + \right.$$
$$\left.\frac{7\cdot 2^{1/7}\Gamma\left(\frac{15}{14}\right)}{\sqrt{\pi}}\left(\frac{31}{4} - 3\xi^2\right)\xi H_{-8/7}(\xi) + \frac{2^{8/7}\Gamma\left(\frac{15}{14}\right)}{\sqrt{\pi}}\left(35 - 12\xi^2\right)H_{-15/7}(\xi)\right]. \tag{3.66}$$

Figure 3.3 provides a plot of this function. Finally, the derivative of the second-order correction is

$$\left.\frac{dC_2}{d\xi}\right|_0 = \frac{3}{121\sqrt{\pi}}\left(\frac{60\Gamma\left(\frac{15}{14}\right)\Gamma\left(\frac{8}{7}\right)}{\Gamma\left(\frac{11}{7}\right)\Gamma\left(\frac{23}{14}\right)} - \frac{469}{8}\right) = 0.12466801... \tag{3.67}$$

at the inner boundary.

3.5 Computation of the flux

Recall that the Ilkovich problem originally asked for the total diffusion-limited molar flowrate to the droplet surface during the drop time. The instantaneous molar flowrate $N(t)$ can be derived from the concentration distribution through Fick's law,

$$N(t) = 4\pi r_0^2 D \left.\frac{\partial c}{\partial r}\right|_{t,r_0}, \tag{3.68}$$

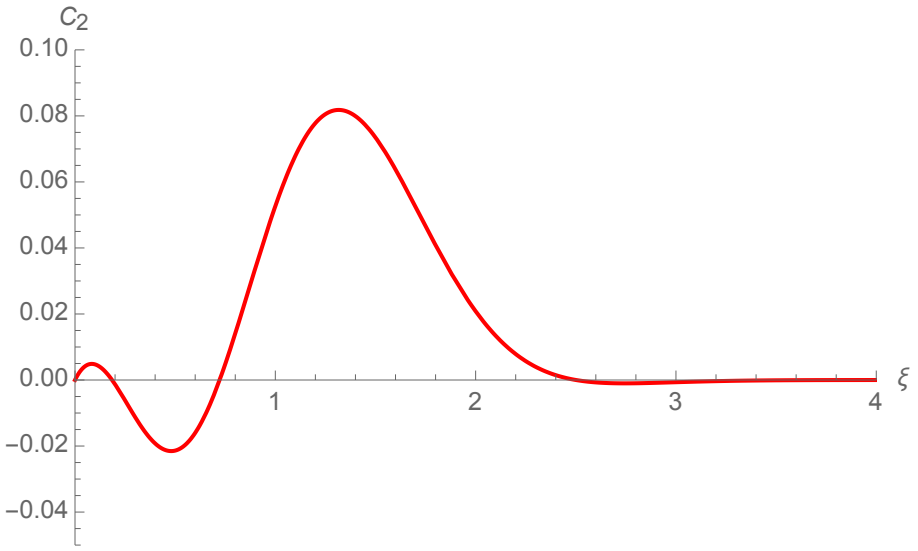

Figure 3.3: Solution for the concentration distribution C_2 from equation 3.66, which satisfies the second-order correction of the Ilkovich model, equation 3.57, with homogeneous boundary conditions at $\xi = 0$ and $\xi \to \infty$. The vertical scale again differs from Figures 3.1 and 3.2.

where a positive concentration gradient is used to make the equation describe flux out of the fluid phase, and a convection term has been excluded because the solute concentration vanishes at the boundary of the droplet. Bringing in C from equation 3.8 and $r_0(t)$ from equation 3.3, and then using equation 3.35 to replace t and r with the dimensionless variables τ and ξ puts equation 3.68 in the form

$$N(\tau) = \frac{7c_\infty Q\tau}{4} \left.\frac{\partial C}{\partial \xi}\right|_{\tau,0}. \tag{3.69}$$

Insertion of the perturbation expansion from equation 3.36, along with the expressions of the derivatives at various orders from equations 3.42, 3.56, and 3.67, shows that the instantaneous flux is given up to the third power of $t^{1/6}$ by equation 3.1, with the constants K_0, K_1, and K_2 given by equation 3.2. In closing, this solution can be connected to prior results. Ilkovich originally reported an equation for flux that was averaged over the drop time t_d, i.e.

$$\frac{1}{t_\mathrm{d}} \int_0^{t_\mathrm{d}} N(t)\, dt = \frac{6K_0}{7} c_\infty Q^{2/3} D^{1/2} t_\mathrm{d}^{1/6} \left[1 + \frac{7K_1}{8}\left(\frac{D^3 t_\mathrm{d}}{Q^2}\right)^{1/6} + \frac{7K_2}{9}\left(\frac{D^3 t_\mathrm{d}}{Q^2}\right)^{1/3} + \ldots\right]. \tag{3.70}$$

With the constants from equation 3.2, one can compute

$$\frac{6K_0}{7} = 3.57232359... \quad \text{and} \quad \frac{7K_1}{8} = 1.45302993...; \tag{3.71}$$

the expression with K_0 is the constant originally stated by Ilkovich, and that with K_1 is the first-order correction reported by Newman. The third constant,

$$\frac{7K_2}{9} = 0.38279341... \tag{3.72}$$

is computed for the first time here. Higher-order terms could be obtained by following the general procedure laid out in the previous section.

3.6 Connection to the Newman-Levich expansion

Newman and Levich perform a more intuitively based analysis of the Ilkovich problem. Although the procedure is more artistic, their method can be shown to produce zeroth, first, and second order corrections consistent with the functions C_0, C_1, and C_2 identified above. Note that Newman introduces a parameter γ, defined as

$$\gamma = \left(\frac{3Q}{4\pi}\right)^{1/3}, \quad \text{or} \quad Q = \tfrac{4}{3}\pi\gamma^3, \tag{3.73}$$

in place of the flowrate Q. The Newman–Levich form of the Ilkovich problem uses independent variables

$$\tau' = \left(\frac{\tau}{2}\right)^{14} = \left(\frac{3D}{7\gamma^2}\right)^7 t^{7/3} \qquad \text{and} \qquad z = 2\xi\left(\frac{\tau}{2}\right)^7 = \frac{r-\gamma t^{1/3}}{\gamma}\left(\frac{3D}{7\gamma^2}\right)^3 t^{2/3}, \tag{3.74}$$

which were presumably identified by the method of undetermined scales. After introducing C in favor of c and substituting these variables for t and r, governing equation 3.5 takes the form

$$\frac{\partial C}{\partial \tau'} - \frac{\partial^2 C}{\partial z^2} = \left\{ \frac{1}{7\tau'^{4/7}}\left[1 - \frac{1}{\left(1+\frac{z}{\tau'^{3/7}}\right)^2} - \frac{2z}{\tau'^{3/7}}\right] + \frac{\frac{z}{\tau'^{3/7}}}{1+\frac{z}{\tau'^{3/7}}} \right\} \frac{\partial C}{\partial z}, \tag{3.75}$$

matching equation 8 of Newman's paper [55]. Terms on the left describe accumulation and diffusion; terms on the right account for convection and the derivative of the scale

factor in the radial part of the spherical Laplacian. The Newman–Levich asymptotics explores a time regime in which the accumulation and diffusion terms of the governing equation are of similar order, and the convection and geometric terms are of higher order. Assuming that C is of order unity, then $\partial C/\partial\tau' = O(\tau'^{-1})$. Since diffusion is expected to be of comparable importance to accumulation, $\partial^2 C/\partial z^2 = O(\tau'^{-1})$ too; because $C = O(1)$ this requires that $z = O(\tau'^{1/2})$. Indeed, Newman comments that "z is of order $\sqrt{\tau'}$ in the boundary layer" [55], although he makes this statement after solving the zero-order problem—presumably because his zero-order result makes the scaling of z clearer. Furthermore, since $z = O(\tau'^{1/2})$, it follows that

$$\frac{z}{\tau'^{3/7}} = \tau'^{1/14} \cdot \frac{z}{\sqrt{\tau'}} = \tau'^{1/14} \cdot O(1) = O(\tau'^{1/14}), \tag{3.76}$$

a relationship that helps to identify the orders of all the terms involving z on the right of equation 3.75. Using the forms $\tau'(\tau, \xi)$ and $z(\tau, \xi)$ from equation 3.74 to replace z with ξ and τ', and subsequently performing a Maclaurin expansion in τ' under the assumption that $\xi = O(1)$, one finds that

$$\left\{ \frac{1}{7\tau'^{4/7}} \left[1 - \frac{1}{\left(1 + \frac{z}{\tau'^{3/7}}\right)^2} - \frac{2z}{\tau'^{3/7}} \right] + \frac{\frac{z}{\tau'^{3/7}}}{1 + \frac{z}{\tau'^{3/7}}} \right\} = \frac{2}{\tau'^{3/7}} \sum_{k=0}^{\infty} (-1)^k \left[1 - \frac{(3+k)\, z^2}{14\tau'} \right] \left(\frac{z}{\tau'^{3/7}} \right)^k \tag{3.77}$$

after some algebraic simplification. Remembering that the kth term of the sum on the right is $O(\tau'^{k/14})$, one can insert this sum into equation 3.75 to show that

$$\frac{\partial C}{\partial \tau'} - \frac{\partial^2 C}{\partial z^2} = \tau'^{-13/14} \left[\left(2 - \frac{3z^2}{z\tau'} \right) - \left(4 - \frac{8z^2}{7\tau'} \right) \frac{z}{2\sqrt{\tau'}} \tau'^{1/14} + O(\tau'^{2/14}) \right] \tau'^{1/2} \frac{\partial C}{\partial z}. \tag{3.78}$$

This explains Newman's statement that the terms neglected by Ilkovich "are of order $\tau'^{-13/14}$ and higher" [55], because the square-bracketed term and $\tau'^{1/2}\partial C/\partial z$ are both $O(1)$. From a formal perspective it may be clearer to consider the form of this equation

obtained after multiplying it through by τ', which yields a result in which the terms on the left of the equals sign are $O(1)$, whereas those on the right are $O(\tau'^{1/14})$.

Following Levich, one can identify a zero-order solution C_0 as the solution of equation 3.78 obtained when its right side is set equal to zero. This problem can be solved by standard methods (Laplace transformation, similarity transformation, etc.), to show that

$$C_0(\tau', z) = -\operatorname{erfc}\left(\frac{z}{2\sqrt{\tau'}}\right) = -1 + \frac{2}{\sqrt{\pi}} \int_0^{\frac{z}{2\sqrt{\tau'}}} e^{-x^2} dx, \tag{3.79}$$

which matches equation 3.41 above, as well as Newman's equation 11 [55].

To get Newman's correction of the Levich–Ilkovich solution, one can perturb C around C_0 to first order (i.e., up to order $\tau'^{1/14}$) and require that the perturbation solve the governing equation obtained by keeping only the first term in square brackets on the right of equation 3.78. One can implement this by supposing that

$$C = C_0 + \theta_1 + O(\tau'^{2/14}). \tag{3.80}$$

Here $C_0 = O(1)$, and we assume that $\theta_1(\tau', z) = O(\tau'^{1/14})$. Noting that $\partial\theta_1/\partial z = O(\tau^{-3/7})$, and inserting the result for C_0, one finds that θ_1 satisfies

$$\frac{\partial\theta_1}{\partial\tau'} - \frac{\partial^2\theta_1}{\partial z^2} = \frac{1}{\sqrt{\pi}} \left(\frac{2}{\tau'^{13/14}} - \frac{3z^2}{7\tau'^{27/14}}\right) \exp\left(-\frac{z^2}{4\tau'}\right), \tag{3.81}$$

which is Newman's equation 13 [55]. After letting

$$\theta_1 = 2\tau'^{1/14} C_1\left(\frac{z}{2\sqrt{\tau'}}\right), \tag{3.82}$$

and after replacing τ' and z with the variables ξ and τ via equation 3.74, one discovers equation 3.43. Thus θ_1 relates directly to the function C_1 reported earlier, in equation 3.55.

The Newman–Levich expansion can be continued to second order by keeping a second term on the right of equation 3.78 and incorporating the results for C_0 and θ_1. Through a similar process this yields the function C_2 given in equation 3.66. Thus

the Newman–Levich method produces results that match those developed in section 3.5 above, although it follows a more circuitous route.

3.7 Numerical approach

A key advantage of the perturbation method developed in section 3.3 is that it produces a sequence of systems of linear ordinary differential equations valid up to arbitrarily high orders. Although the analytical techniques from section 3.4 are easily extended in principle, the process of solving these systems of equations becomes increasingly arduous as the order of the perturbation increases. It will be worthwhile to check the solutions of the regularly perturbed problem against numerical results, to see when higher-order corrections beyond those of Ilkovich and Newman are needed.

Another motivation for a numerical approach is that some assumptions underpinning our analysis do not always hold. In section 3.3, the regular perturbation in time hinges on Maclaurin expansions of the coefficients in governing equation 3.3. Such expansions require that $\eta \mathrm{T}^{1/6} < 1$ (or $\xi\tau < 1$) so that the two series in equation 3.25 lie within their radii of convergence. Recalling that we are interested in a concentration boundary layer, where η (or ξ) is of order unity, use of these series restricts the analysis to situations where $\mathrm{T} < 1$ (or $\tau < 1$). The reader should be aware that dimensionless drop times of order unity can be accessed by perfectly reasonable experimental polarography systems: for example, if $D = 5 \cdot 10^{-5}$ cm$^2\, s^{-1}$, $t_\mathrm{d} = 15$ s, and the droplet diameter at t_d is 0.075 cm, equation 3.18 yields a dimensionless drop time of ~ 1.4. In this regime of τ, one must be wary of using the short-time asymptotic expansion.

Because the Ilkovich problem contains no free parameters, an accurate numerical solution is worth pursuing anyway. Any numerical results obtained for how flux depends on time are universal, and can be carried to any regime of τ. From this philosophical perspective, asymptotic formulas valid at small τ simply help to verify

numerical methods. Once short-time results have been verified up to the desired precision, a numerical computation can readily be extended into the regime where the regular perturbation discussed above no longer works. One might attempt a matched asymptotic expansion to get analytical traction on the large-time problem, but it is debatable whether this would yield insight or precision superior to a purely numerical plan of attack.

Numerics are not a panacaea, however. The ostensible simplicity of the dimensionless problem posed by equations 3.9-3.11 belies some serious barriers to accurate computation of solutions. First, the time-varying radial boundary in BCi makes spatial meshing difficult. Second, the involvement of a growing concentration boundary layer, which is extremely thin at small times, necessitates a relationship between the durations of the time stepping and the fineness of the spatial resolution. A coordinate transformation that makes BCi stationary yields the system of equations 3.15-3.17. Unfortunately, this formulation does not alleviate the numerical challenge, but instead moves it to another part of the equation system. The time dependence on the right in equation 3.15 makes GE ill conditioned, and consequently highly error prone, at short times.

The asymptotics and perturbation analysis in section 3.3 suggest a route to circumvent the numerical difficulties posed by equation systems 3.9-3.11 and 3.15-3.17. Instead of solving either of these systems, we instead solve a transformed version of the problem that includes the information gained from short-time asymptotics, but does not employ the Maclaurin expansion used for the perturbation.

A numerically amenable transformed governing equation is found by letting $\alpha = 1/6$ in equation 3.3, exchanging the independent variables η and T for ξ and τ through definitions 3.31, and then rearranging terms so that the differential operator from equation 3.37 appears on the left side of the equality. Next, a more stable initial condition is identified by recognizing that the expression of $C_0(\xi)$ from equation 3.41

satisfies the requirements of the IC from equation 3.33, while also satisfying GE, BCi, and BCii at $\tau = 0$. Thus one arrives at the equation system

$$\text{GE:}\quad \frac{\partial^2 C}{\partial \xi^2} + 2\xi \frac{\partial C}{\partial \xi} = \frac{2\tau}{7}\left\{\frac{\partial C}{\partial \tau} + \frac{\left[2\xi^2 + (1+\xi\tau)\left(4\xi^2 - 7\right)\right]}{(1+\xi\tau)^2}\frac{\partial C}{\partial \xi}\right\} \tag{3.83}$$

$$\text{IC:}\quad C(0,\xi) = -\operatorname{erfc}(\xi) \tag{3.84}$$

$$\text{BCi:}\quad C(\tau,0) = -1 \qquad \text{BCii:}\quad C(\tau,\infty) = 0, \tag{3.85}$$

which can be used to find accurate numerical solutions. The terms on the right of GE are of order τ or higher in the neighborhood of $\tau = 0$, as can be verified by observing that Maclaurin expanding the right side of GE with respect to τ produces equation 3.32.

To solve equation system 3.83-3.85, a numerical simulation was performed using finite elements with Firedrake software [58], using the MUMPS direct linear solver [59, 60] via PETSc [61, 62]. The spatial discretization consisted of continuous piecewise second order polynomials on 10,000 equispaced grid points on the interval $\xi \in [0, 5]$ and the time discretization used the implicit first-order Euler scheme with 1000 timesteps in the interval $\tau \in [0, 1]$. Exploiting piecewise polynomial functions in the discretization of the problem allows for a straightforward computation of the derivative $\partial C/\partial \xi$ at $\xi = 0$ at each time step.

The instantaneous flux to the droplet surface depends on concentration derivatives at the droplet surface through equation 3.69. Taking the perturbation analysis up to nth order yields an approximate expression for these derivatives,

$$\left.\frac{\partial C}{\partial \xi}\right|_{\tau,0} \approx \sum_{k=0}^{n} \left.\frac{dC_k}{d\xi}\right|_0 \tau^k, \tag{3.86}$$

with the coefficients at noughth, first, and second order on the right given respectively by equations 3.42, 3.56, and 3.67. Figure 3.4a compares the derivative at the surface computed numerically via Firedrake with the approximations yielded by the analyses of Ilkovich ($n = 0$ in equation 3.86) and Newman ($n = 1$), as well as the results developed in sections 3.3 and 3.4 ($n = 2$).

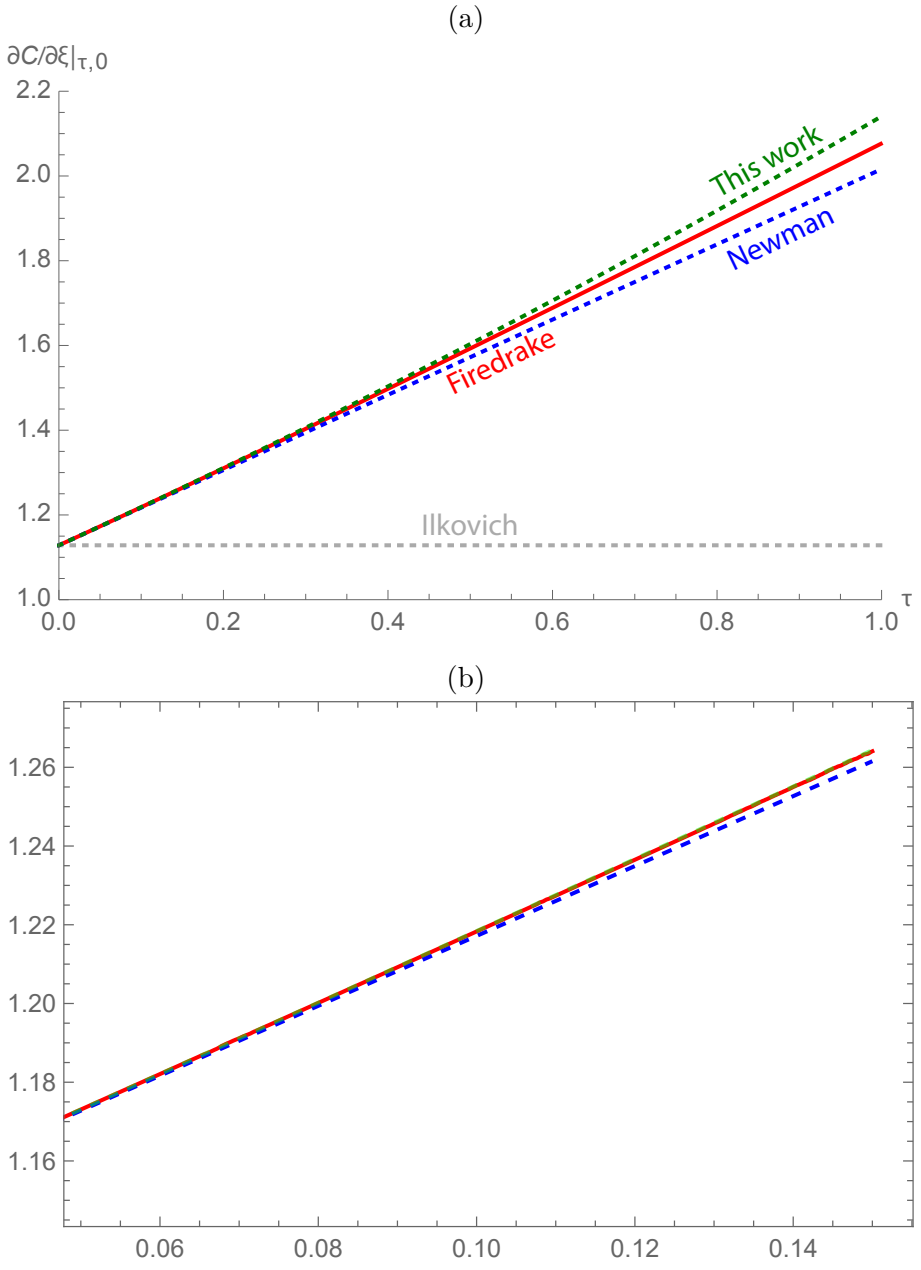

Figure 3.4: (a) Dimensionless spatial concentration gradients at the droplet surface, $\partial C/\partial \xi|_{\tau,0}$, computed numerically by solving equations 3.83-3.85 with the Firedrake finite-element software (red) alongside the analytical approximations from Ilkovich (gray dashed), Newman (blue dashed), and this work (green dashed). (b) Zoomed in figure showing second-order correction matching with the numerical result for $\tau < 0.15$.

Ilkovich's approximate solution deviates rapidly from the numerical solution; the two only match at $\tau = 0$. Newman's solution broadly captures the time dependence of $(\partial C/\partial \xi)|_{\tau,0}$ at short times, matching the numerical result within 0.1% for $\tau < 0.05$, then deviating increasingly positively from it. The second-order correction extends this domain, matching the numerical result within 0.1% for $\tau < 0.15$.

Higher corrections impact values of the concentration derivative far more than they affect Ilkovich's equation, because Ilkovich's equation models the average flux over the drop time, rather than instantaneous flux. Through the definition of a dimensionless average flux, $\langle N \rangle_{t_d}$, as

$$\langle N \rangle_{t_d} = \frac{1}{t_d} \int_0^{t_d} 4N\,(t) dt = \frac{21 Q c_\infty}{2\tau_d^6} \int_0^{\tau_d} \tau^6 \left. \frac{\partial C}{\partial \xi} \right|_{\tau,0} d\tau, \tag{3.87}$$

the essential content of the Ilkovich equation can be cast dimensionlessly. The sixth power to which τ is raised in the integral at right makes the error of asymptotic formulas for the average flux behave somewhat differently than the error in the concentration derivative.

To get a numerical expression of $\langle N \rangle_{t_d}$, the integral on the right of equation 3.87 was calculated by applying an explicit second-order backward difference formula to the integrand, which was calculated at each τ using the numerical results for $\frac{\partial C}{\partial \xi}|_{\tau,0}$. Figure 3.5b compares this result to the original Ilkovich equation, as well as the corrected forms developed by Newman and in sections 3.3 and 3.4. Both the first and second-order corrections approximate the true solution of the problem much more accurately than the Ilkovich formula, which deviates rapidly from the numerical solution. Newman's approximation deviates by less than 0.1% from Firedrake up to $\tau = 0.12$. The second-order correction of Ilkovich's equation improves on this, agreeing with the Firedrake result within 0.1% up to dimensionless times of $\tau = 0.27$. Still, the averaging approach makes the impact of higher-order corrections relatively marginal. At $\tau = 1$, Newman's first-order result underpredicts the numerical calcu-

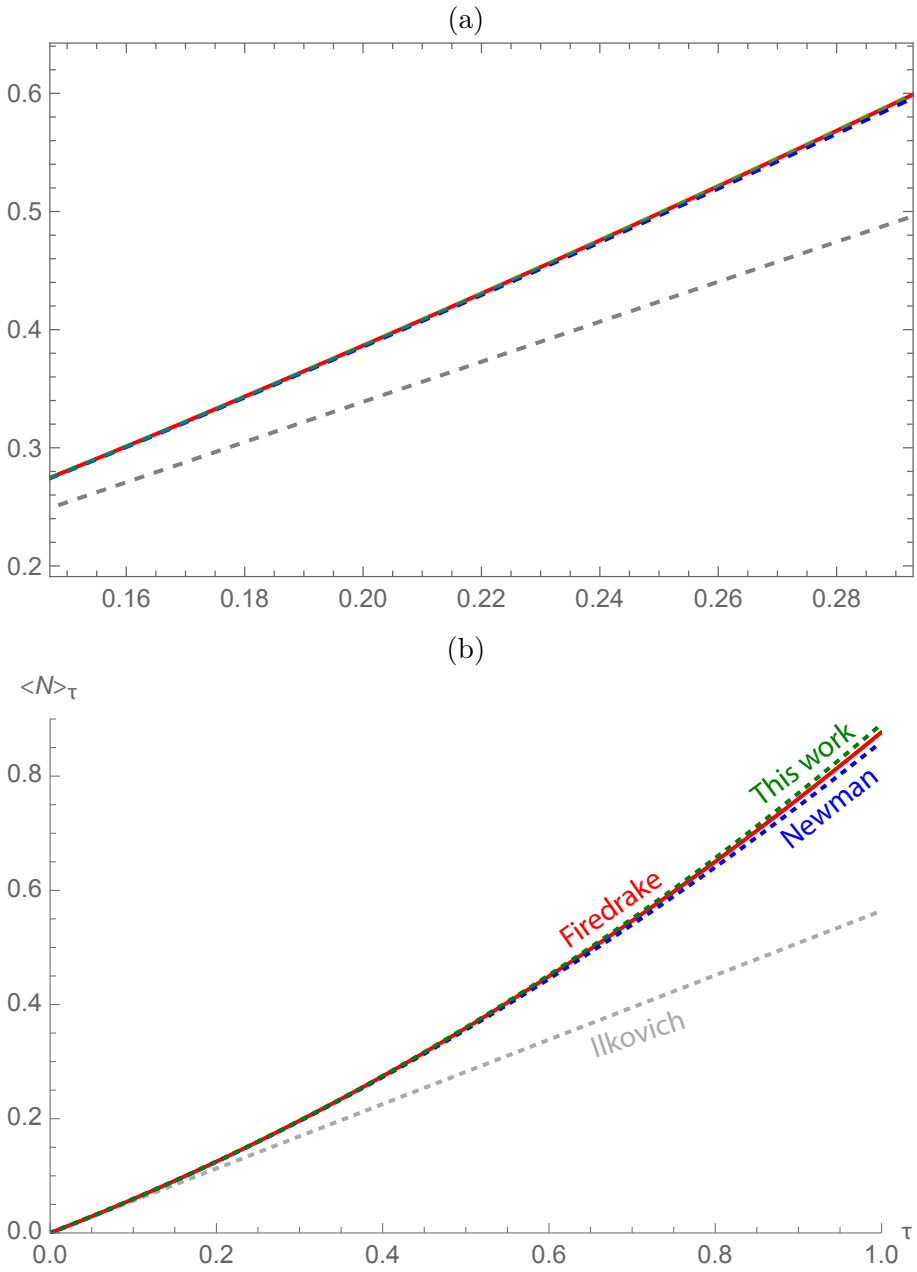

Figure 3.5: (a) Zoomed in figure. (b) Dimensionless net flux averaged over the dimensionless drop time, $\langle N \rangle_\tau$, computed using the Firedrake finite-element software (red), compared to the classical Ilkovich result (gray dashed), the first-order correction by Newman (blue dashed), and the second-order correction from this work (green dashed).

Table 3.1: Comparison between different estimated values of the diffusion coefficient in the revised Ilkovic equation.

Model	Nominal Parameter	Estimated Parameter	95% C.I.
Ilkovic	5.0×10^{-9}	1.0209×10^{-8}	1.4329×10^{-10}
Newman	5.0×10^{-9}	5.1045×10^{-9}	1.6542×10^{-11}
This work	5.0×10^{-9}	4.9390×10^{-9}	1.5744×10^{-11}

lation by 2.5%, whereas the present, second-order, result overpredicts the numerics by 2.4%.

3.8 Analysis of Polorographic data

In order to estimate values of the diffusion coefficient using the Ilkovic, Newman, and the present models, a zero mean Gaussian noise with the specified standard deviation (0.01) is added to the data obtained by running the rigorous numerical model. The data consists of the instantaneous current during the life of a drop. The parameters used to generate the data are: maximum diameter of the droplet is 0.1 cm, drop time $t_{\mathrm{d}} = 10s$, and the diffusivity of solute is $5 \cdot 10^{-5} cm^2 s^{-1}$.

Table 3.1 lists the diffusion coefficient values obtained by fitting the data using the classical Ilkovich result, the first-order correction by Newman, and the second-order correction from this work. For comparison, in diffusion coefficients from the Ilkovic equation without the last two terms, the diffusion coefficient was higher than the nominal parameter by approximately 100%, and those for the Newman equation without the last term and the current work were higher by about 2% and 1%, respectively. 95% Confidence intervals are calculated to provide an accuracy range for the estimated parameters. The results indicate that this work has narrow confidence intervals, while Ilkovic has relatively wide confidence intervals. This finding is intuitive since large variations in the parameters using Ilkovic produce trivial changes in the instantaneous current output trajectory.

Figure 3.6 presents the results obtained by fitting the data to the original Ilkovich

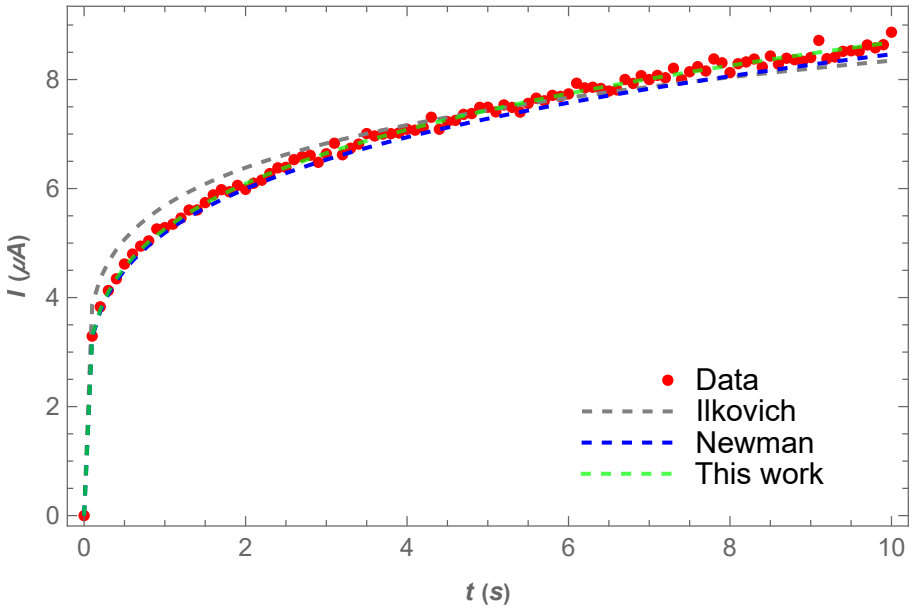

Figure 3.6: Instantaneous current data (red circles) during the life of a drop fitted to the classical Ilkovich result (gray dashed), the first-order correction by Newman (blue dashed), and the second-order correction from this work (green dashed).

equation, the corrected forms developed by Newman, and in sections 3.3 and 3.4. The agreement between data and theory has become better: the deviation at $t = 10s$ being only 1% for the second order correction, 4.5% for the first order, and 5.9% for the zeroth order. Thus it is concluded that the second term may not always be negligible.

3.9 Conclusion

The classical Ilkovich equation works robustly to describe the polarographic response of relatively slow-diffusing solutes when drop times are short and falling droplets are relatively large. In cases where these conditions are not met diffusion is fast, drop times are long, or terminal drop sizes are smaller our analysis showed that high-erorder corrections may be needed. We found that Newman's first-order correction and our second-order correction of the Ilkovich equation both track an ostensibly exact numerical solution of the Ilkovich problem within a few percent. The second

order correction we developed in Section 4 matches the numerical solution computed with Firedrake software in Section 7 within 0.1% when the dimensionless drop time τ_d, related to the true drop time t_d through Eq. 3.35, is less then 0.27 about twice the range where Newman's approximation is similarly accurate. Whereas the classical Ilkovich equation becomes inaccurate at extremely small dimensionless drop times, Newman's correction and our correction both predict the numerically calculated true solution of the Ilkovich problem within 2-3% across a wide range of dimensionless drop times (up to at least $\tau_d = 1$). The error in both the first-order correction by Newman and our second-order correction is probably comparable to or smaller than the intrinsic error of most polarography experiments. Thus Newman's correction suffices for most applications. Nevertheless, the asymptotic approaches presented here can be usefully applied to develop robust approaches to various physical extensions of the original Ilkovich problem. Possible model extensions include the determination of surface flux in response to potential sweeps rather than potential steps, or accounting for interfacial capacitance and reaction overpotential in the system response.

Chapter 4

Analytical solutions for boundary value problems

4.1 Introduction

Using analytical solutions in chemical engineering education helps students who make quantitative predictions. One of the main reasons is that analytical solutions are exact solutions. This guarantees that the resulting quantitative predictions are accurate. We present here an analytical solution method using Maple to solve systems of second-order linear ordinary differential equations in single and multiple domains. We start by reducing the order of the differential equations by assuming that the first-order derivative is an additional dependent variable [63]. This reduction yields a set of linear first-order differential equations that includes all the dependent variables (e.g., concentration), the first-order derivatives of the dependent variables (e.g., flux), and the parameters of the system. These equations can be solved by finding the matrix exponential [64] and symbolically integrating the resulting system of equations using Maple. Our method is similar to our previously presented analytical method for solving initial value problems (IVPs) [65]. The method presented here is an extension to the previous method and is valid for various boundary conditions and constraints for boundary value problems (BVPs) in single and multiple domains. First, the methodology is illustrated using a general second order linear differential equation with generalized boundary conditions. Once the solution is obtained, we explain how the this solution can be used to generate solutions for linear problems

from chemical engineering for different boundary conditions [66]. Next, the methodology for solving boundary value problems with boundary conditions that require an additional constraint is illustrated by solving a boundary value problem with similar flux conditions at the boundaries in a lithium/polymer battery cell [67]. Finally, we demonstrate the methodology for a similar BVP with multiple domains that requires a multiple domain constraint equation by solving the coupled equations for the steady-state analysis of a lithium/polymer cell under uniform current distribution [68], and we used COMSOL to verify our solution. We present the model equations and their solutions in the body of our paper and the Maple solutions are available upon request from the authors.

4.2 Analytical method for linear ordinary differential equations (ODEs)

For the second order linear ODE of the following form:

$$\frac{d^2\theta}{dx^2} + p\frac{d\theta}{dx} + q\theta = f(x) \tag{4.1}$$

and the following boundary conditions

$$k_1\frac{d\theta}{dx} + h_1\theta = 0, \quad \text{at} \quad x = 0 \tag{4.2}$$

$$k_2\frac{d\theta}{dx} + h_2\theta = 0, \quad \text{at} \quad x = 1 \tag{4.3}$$

Let $y_1 = \theta$, and $y_2 = \frac{d\theta}{dx}$, so that the governing equation can be transformed into the following equation system:

$$\frac{dy_1}{dx} - y_2 = 0 \tag{4.4}$$

$$\frac{dy_2}{dx} + py_2 + qy_1 = f(x) \tag{4.5}$$

Equation 4.4-4.5 can be written in matrix form:

$$\frac{d\underline{\mathbf{Y}}}{dx} + \underline{\underline{\mathbf{A}}}\ \underline{\mathbf{Y}} = \underline{\mathbf{b}}(x) \tag{4.6}$$

where $\underline{\mathbf{Y}} = \begin{bmatrix} y_1 \\ y_2 \end{bmatrix}$, $\underline{\underline{\mathbf{A}}} = \begin{bmatrix} 0 & -1 \\ q & p \end{bmatrix}$, and $\underline{\mathbf{b}}(x) = \begin{bmatrix} 0 \\ f(x) \end{bmatrix}$. Let $\underline{\mathbf{Y}}_0 = \underline{\mathbf{Y}}|_{x=0}$, and $\underline{\mathbf{Y}}_1 = \underline{\mathbf{Y}}|_{x=1}$, so that the boundary conditions can be writtten as

$$\underline{\underline{\mathbf{C}}}\ \underline{\mathbf{Y}}_0 + \underline{\underline{\mathbf{D}}}\ \underline{\mathbf{Y}}_1 = \underline{\mathbf{Bc}} \tag{4.7}$$

where $\underline{\underline{\mathbf{C}}} = \begin{bmatrix} h_1 & k_1 \\ 0 & 0 \end{bmatrix}$, $\underline{\underline{\mathbf{D}}} = \begin{bmatrix} 0 & 0 \\ h_2 & k_2 \end{bmatrix}$, and $\underline{\mathbf{Bc}} = \begin{bmatrix} c_1 \\ c_2 \end{bmatrix}$. The general form of the solution of equation 4.6 is

$$\underline{\mathbf{Y}} = \exp\left(-\underline{\underline{\mathbf{A}}}x\right)\underline{\mathbf{Y}}_0 + \int_0^x \exp\left[-\underline{\underline{\mathbf{A}}}(x-\lambda)\right]\underline{\mathbf{b}}(\lambda)\,d\lambda \tag{4.8}$$

where λ is a dummy variable in integration. The matrix exponential [64] of a square matrix (i.e., $\exp(\underline{\underline{\mathbf{A}}})$) can be expressed by Taylor expression given by

$$\exp\left(\underline{\underline{\mathbf{A}}}\right) = \underline{\underline{\mathbf{I}}} + \frac{1}{1!}\underline{\underline{\mathbf{A}}} + \frac{1}{2!}\underline{\underline{\mathbf{A}}}^2 + \frac{1}{3!}\underline{\underline{\mathbf{A}}}^3 + ... \tag{4.9}$$

where $\underline{\underline{\mathbf{I}}}$ is the identity matrix with same dimensions as $\underline{\underline{\mathbf{A}}}$. Equation 4.8 yields at $x = 1$,

$$\underline{\mathbf{Y}}_1 = \exp\left(-\underline{\underline{\mathbf{A}}}\right)\underline{\mathbf{Y}}_0 + \underline{\mathbf{F}} \tag{4.10}$$

where $\underline{\mathbf{F}} = \int_0^1 \exp\left[-\underline{\underline{\mathbf{A}}}(1-\lambda)\right]\underline{\mathbf{b}}(\lambda)\,d\lambda$. Next, substitute equation 4.10 into equation 4.7 to obtain

$$\underline{\underline{\mathbf{C}}}\ \underline{\mathbf{Y}}_0 + \underline{\underline{\mathbf{D}}}\ \left[\exp\left(-\underline{\underline{\mathbf{A}}}\right)\underline{\mathbf{Y}}_0 + \underline{\mathbf{F}}\right] = \underline{\mathbf{Bc}} \tag{4.11}$$

From equation 4.11 we obtain

$$\underline{\mathbf{Y}}_0 = \left[\underline{\underline{\mathbf{C}}} + \underline{\underline{\mathbf{D}}}\exp\left(-\underline{\underline{\mathbf{A}}}\right)\right]^{-1}\left(\underline{\mathbf{Bc}} - \underline{\underline{\mathbf{D}}}\ \underline{\mathbf{F}}\right) \tag{4.12}$$

Now, substitute equation 4.12 into equation 4.8 to get the solution

$$\underline{\mathbf{Y}} = \exp\left(-\underline{\underline{\mathbf{A}}}x\right)\left[\underline{\underline{\mathbf{C}}} + \underline{\underline{\mathbf{D}}}\exp\left(-\underline{\underline{\mathbf{A}}}\right)\right]^{-1}\left(\underline{\mathbf{Bc}} - \underline{\underline{\mathbf{D}}}\ \underline{\mathbf{F}}\right) + \int_0^x \exp\left[-\underline{\underline{\mathbf{A}}}(x-\lambda)\right]\underline{\mathbf{b}}(\lambda)\,d\lambda \tag{4.13}$$

Thus, an analytical solution is obtained for the general linear second order differential equation and boundary conditions. Equations 4.1-4.13 can be modeled easily in Maple.

Example 1: Irreversible Homogeneous Reaction in a Liquid

We demonstrate the method for linear problems by solving a general diffusion equation from chemical engineering. Consider the first order, irreversible conversion of species A to B in a stationary liquid film. The governing differential equation [66], page 54-56, in dimensionless form

$$\frac{d^2\theta}{d\eta^2} - Da\theta = 0 \tag{4.14}$$

subject to the following boundary conditions,

$$\frac{d\theta}{d\eta}(0) = 0 \tag{4.15}$$

$$\theta(1) = 1 \tag{4.16}$$

where θ is the dimensionless concentration, η is the dimensionless distance and Da is the Damköhler number for reaction relative to diffusion. The stationary liquid film is chosen because it is linear and has an analytical solution:

$$\theta(\eta) = \frac{\cosh\left(\sqrt{Da}\eta\right)}{\cosh\left(\sqrt{Da}\right)} \tag{4.17}$$

Equation 4.14 can be written in the form of a vector differential equation 4.6, where

$$\underline{\mathbf{Y}} = \begin{bmatrix} y_1 \\ y_2 \end{bmatrix} = \begin{bmatrix} \theta \\ \frac{d\theta}{dx} \end{bmatrix} \tag{4.18}$$

$$\underline{\underline{\mathbf{A}}} = \begin{bmatrix} 0 & -1 \\ -Da & 0 \end{bmatrix} \tag{4.19}$$

$$\underline{\underline{\mathbf{C}}} = \begin{bmatrix} 0 & 1 \\ 0 & 0 \end{bmatrix}, \quad \underline{\underline{\mathbf{D}}} = \begin{bmatrix} 0 & 0 \\ 1 & 0 \end{bmatrix} \quad \text{and} \quad \underline{\mathbf{Bc}} = \begin{bmatrix} 0 \\ 1 \end{bmatrix} \tag{4.20}$$

The general solution presented in equation 4.13 is valid for this BVP. For this example, the coefficient matrix $\underline{\underline{\mathbf{A}}}$ equation 4.19 is constant since Da is constant $\underline{\mathbf{F}}$ and forcing function $\underline{\mathbf{b}}(\mathrm{t})$ are zero. Therefore equation 4.13 simplifies to the following equation:

$$\underline{\mathbf{Y}} = \exp\left(-\underline{\underline{\mathbf{A}}}x\right)\left[\underline{\underline{\mathbf{C}}} + \underline{\underline{\mathbf{D}}}\exp\left(-\underline{\underline{\mathbf{A}}}\right)\right]^{-1}(\underline{\mathbf{Bc}}) \tag{4.21}$$

Hence, by substituting equations 4.19, 4.20 into equation 4.21 we get,

$$\underline{\mathbf{Y}} = \begin{bmatrix} y_1 \\ y_2 \end{bmatrix} = \begin{bmatrix} \theta \\ \frac{d\theta}{dx} \end{bmatrix} = \begin{bmatrix} \frac{\exp\left(\sqrt{Da}\eta\right)+\exp\left(-\sqrt{Da}\eta\right)}{\exp\left(\sqrt{Da}\right)+\exp\left(-\sqrt{Da}\right)} \\ \frac{\sqrt{Da}\exp\left(\sqrt{Da}\eta\right)+\sqrt{Da}\exp\left(-\sqrt{Da}\eta\right)}{\exp\left(\sqrt{Da}\right)+\exp\left(-\sqrt{Da}\right)} \end{bmatrix} \tag{4.22}$$

From the first row of the matrix equation 4.22 θ is obtained as,

$$\theta = \frac{\exp\left(\sqrt{Da}\eta\right)+\exp\left(-\sqrt{Da}\eta\right)}{\exp\left(\sqrt{Da}\right)+\exp\left(-\sqrt{Da}\right)} = \frac{\cosh\left(\sqrt{Da}\eta\right)}{\cosh\left(\sqrt{Da}\right)} \tag{4.23}$$

which is same as equation 4.17. The solution obtained using matrix exponential is plotted in Figure 4.1 with Da as a parameter.

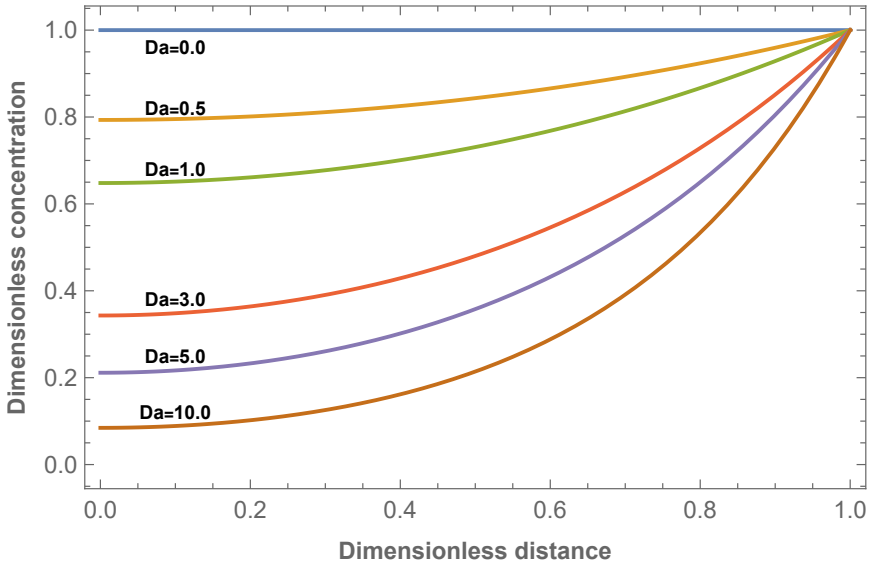

Figure 4.1: Dimensionless concentration profiles in a stationary liquid film as a function of Damköhler number.

Example 2: Reversible Homogeneous Reaction in a Liquid

Consider the reversible conversion of species A to B in a stationary liquid film. The governing differential equations [66], page 57-59, are

$$D_A \frac{d^2 C_A}{dy^2} + k_{-1} C_B - k_1 C_A = 0, \quad D_B \frac{d^2 C_B}{dy^2} - k_{-1} C_B + k_1 C_A = 0 \tag{4.24}$$

subject to the following boundary conditions

$$C_A(0) = C_{A0}, \quad C_B(0) = C_{B0} \tag{4.25}$$

$$\frac{dC_A}{dy}(L) = 0, \quad \frac{dC_B}{dy}(L) = 0 \tag{4.26}$$

Using the dimensionless variables

$$\eta = \frac{y}{L}, \quad \theta_A = \frac{C_A}{C_{A0}}, \quad \theta_B = \frac{KC_B}{C_{A0}}, \quad K = \frac{k_{-1}}{k_1} \tag{4.27}$$

Equation 4.24 converts to

$$\frac{d^2 C_A}{d\eta^2} + \frac{L^2}{D_A}(k_{-1} C_B - k_1 C_A) = 0, \quad \frac{d^2 C_B}{d\eta^2} - \frac{L^2}{D_B}(k_{-1} C_B - k_1 C_A) = 0 \tag{4.28}$$

or

$$\frac{1}{C_{A0}} \frac{d^2 C_A}{d\eta^2} + \frac{k_1 L^2}{D_A}\left(\frac{k_{-1} C_B}{k_1 C_{A0}} - \frac{C_A}{C_{A0}}\right) = 0, \quad \frac{1}{C_{A0}} \frac{d^2 C_B}{d\eta^2} - \frac{k_{-1} L^2}{D_B}\left(\frac{C_B}{C_{A0}} - \frac{k_1 C_A}{k_{-1} C_{A0}}\right) = 0 \tag{4.29}$$

Let the dimensionless parameters be

$$\alpha = \frac{k_1 L^2}{D_A}, \quad \beta = \frac{k_{-1} L^2}{D_B}, \quad \gamma = \frac{KC_{B0}}{C_{A0}} \tag{4.30}$$

Equation 4.29 then converts to

$$\frac{d^2 \theta_A}{d\eta^2} + \alpha(\theta_B - \theta_A) = 0, \quad \frac{d^2 \theta_B}{d\eta^2} - \beta(\theta_B - \theta_A) = 0 \tag{4.31}$$

Boundary conditions 4.25, 4.26 then convert to

$$\theta_A(0) = 1, \quad \theta_B(0) = \gamma \tag{4.32}$$

$$\frac{d\theta_A}{d\eta}(1) = 0, \quad \frac{d\theta_B}{d\eta}(1) = 0 \tag{4.33}$$

The final solution for this case can be obtained by substituting $\underline{\underline{\mathbf{A}}} = \begin{bmatrix} 0 & 0 & -1 & 0 \\ 0 & 0 & 0 & -1 \\ -\alpha & \alpha & 0 & 0 \\ \beta & \beta & 0 & 0 \end{bmatrix}$, $\underline{\underline{\mathbf{C}}} = \begin{bmatrix} 1 & 0 & 0 & 0 \\ 0 & 1 & 0 & 0 \\ 0 & 0 & 0 & 0 \\ 0 & 0 & 0 & 0 \end{bmatrix}$, $\underline{\underline{\mathbf{D}}} = \begin{bmatrix} 0 & 0 & 0 & 0 \\ 0 & 0 & 0 & 0 \\ 0 & 0 & 1 & 0 \\ 0 & 0 & 0 & 1 \end{bmatrix}$, $\underline{\mathbf{b}} = \begin{bmatrix} 0 \\ 0 \\ 0 \\ 0 \end{bmatrix}$ and $\underline{\mathbf{Bc}} = \begin{bmatrix} 1 \\ \gamma \\ 0 \\ 0 \end{bmatrix}$ into equation 4.13. For brevity, the final solution is not given here. Instead, the steady-state concentration profiles in a liquid film with a reversible homogeneous reaction are plotted in Figure 4.2.

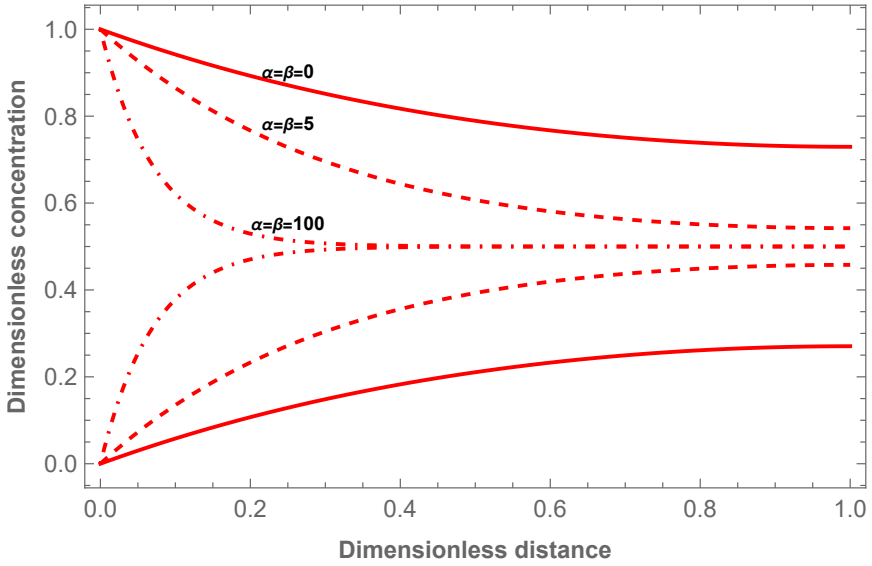

Figure 4.2: Reactant concentrations for steady diffusion in a liquid film with a reversible homogeneous reaction. In all three cases $\gamma = 0$; consequently, the top curves are for species A.

Example 3: Jump Condition for Dopant Concentration C at a Melt/Crystal Interface

Consider a continuous solidification process. The governing differential equation [66], page 64-66, is,

$$D\frac{d^2C}{dx^2} - U\frac{dC}{dx} = 0 \tag{4.34}$$

$$C_s = KC\left(\delta\right) \tag{4.35}$$

with the boundary conditions

$$C\left(0\right) = C_\infty \tag{4.36}$$

$$UC\left(\delta\right) - D\frac{dC}{dx}\left(\delta\right) = UC_s \tag{4.37}$$

Using equation 4.35 to eliminate C_s from equation 4.37, the interfacial balance becomes

$$U\left(1-K\right)C\left(\delta\right) - D\frac{dC}{dx}\left(\delta\right) = 0 \tag{4.38}$$

The final solution for this case can be obtained by substituting $\underline{\underline{\mathbf{A}}} = \begin{bmatrix} 0 & -1 \\ 0 & -\frac{U}{D} \end{bmatrix}$, $\underline{\underline{\mathbf{C}}} = \begin{bmatrix} 1 & 0 \\ 0 & 0 \end{bmatrix}$, $\underline{\underline{\mathbf{D}}} = \begin{bmatrix} 0 & 0 \\ U\left(1-K\right) & -D \end{bmatrix}$, $\underline{\mathbf{b}} = \begin{bmatrix} 0 \\ 0 \end{bmatrix}$, and $\underline{\mathbf{Bc}} = \begin{bmatrix} C_\infty \\ 0 \end{bmatrix}$ into equation 4.13. Hence the analytical solution of equation 4.34 that satisfies boundary conditions 4.36 and 4.38 is

$$C\left(y\right) = C_\infty \frac{K + (1-K)e^{\frac{(x-\delta)U}{D}}}{K + (1-K)e^{\frac{-U\delta}{D}}} \tag{4.39}$$

Equation 4.39 can be rewritten using dimensionless parameters $\theta = \frac{C}{C_\infty}$, $\eta = \frac{y}{\delta}$ and $Pe = \frac{U\delta}{D}$ as

$$\theta\left(\eta\right) = \frac{K + (1-K)e^{Pe(\eta-1)}}{K + (1-K)e^{-Pe}} \tag{4.40}$$

where Pe is the Peclet number for the dopant. The profiles obtained for $Pe = 5$ and $K = 0.8$ are plotted in Figure 4.3.

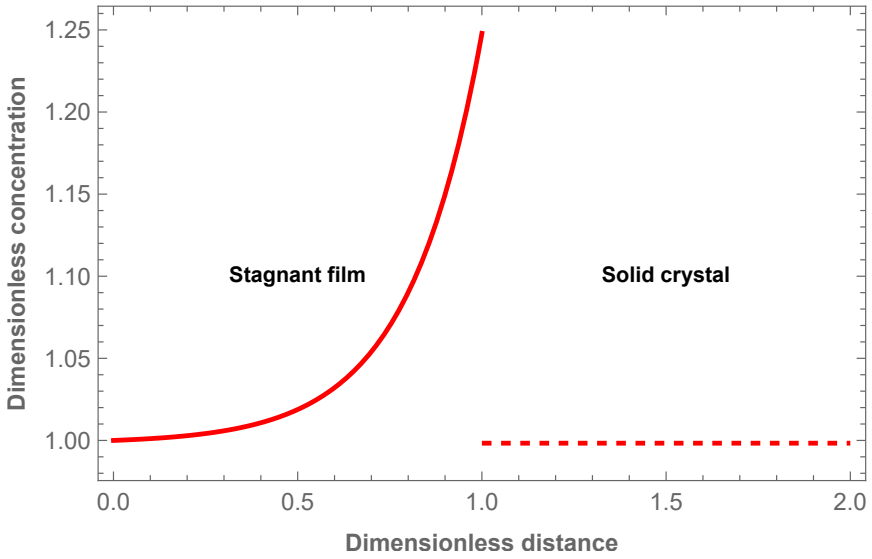

Figure 4.3: Dopant concentrations for steady diffusion in a stagnant film and in a solid crystal.

Example 4: Monroe and Newman Dendrite Growth Model: Steady State Solution

Monroe and Newman [67] presented a dendrite growth model in a parallel electrode lithium/polymer cell during galvanostatic charging. The steady state concentration profiles in their cell (see their figure 1) is given by

$$D\frac{d^2c}{dx^2} = 0 \tag{4.41}$$

with the boundary condition

$$\frac{dc}{dx} = \frac{-i\left(1-t_+^0\right)}{DF}, \qquad @ \qquad x = 0 \tag{4.42}$$

and the constraint equation

$$\int_0^L c\left(x\right)dx = c_b L \tag{4.43}$$

Note that the boundary condition at $x = L$ would be the same as equation 4.42 with a positive sign and would consequently not provide sufficient information to obtain a solution. Instead, we must invoke conservation of mass or moles in this case since there is no homogeneous reaction. The constraint equation for this model, equation

4.43, expresses conservation of mass or moles in this case. Now let $y_1 = c$ and $y_2 = \frac{dc}{dx}$, and the governing equation becomes the following equation system

$$\frac{dy_1}{dx} = y_2 \tag{4.44}$$

$$\frac{dy_2}{dx} = 0 \tag{4.45}$$

Rewrite equations 4.44 and 4.45

$$\frac{d}{dx}\begin{bmatrix} y_1 \\ y_2 \end{bmatrix} + \begin{bmatrix} 0 & -1 \\ 0 & 0 \end{bmatrix}\begin{bmatrix} y_1 \\ y_2 \end{bmatrix} = \begin{bmatrix} 0 \\ 0 \end{bmatrix} \tag{4.46}$$

Let $\underline{\mathbf{Y}} = \begin{bmatrix} y_1 \\ y_2 \end{bmatrix}$, $\underline{\underline{\mathbf{A}}} = \begin{bmatrix} 0 & -1 \\ 0 & 0 \end{bmatrix}$, and $\underline{\mathbf{b}} = \begin{bmatrix} 0 \\ 0 \end{bmatrix}$, the equation system can be expressed with the matrix format

$$\frac{d\underline{\mathbf{Y}}}{dx} + \underline{\underline{\mathbf{A}}}\,\underline{\mathbf{Y}} = \underline{\mathbf{b}} \tag{4.47}$$

The general form of the solution is obtained from equation 4.47

$$\underline{\mathbf{Y}} = \exp\left(-\underline{\underline{\mathbf{A}}}x\right)\underline{\mathbf{Y}}_0 + \int_0^x \exp\left[-\underline{\underline{\mathbf{A}}}\,(x-\lambda)\right]\underline{\mathbf{b}}d\lambda \tag{4.48}$$

Let $\underline{\mathbf{Y}}_0 = \underline{\mathbf{Y}}|_{x=0}$ and $\underline{\mathbf{Y}}_c = \int_0^L \underline{\mathbf{Y}}dx$ and obtain

$$\underline{\mathbf{Y}}_c = \int_0^L \underline{\mathbf{Y}}dx = \int_0^L \exp\left(-\underline{\underline{\mathbf{A}}}x\right)\underline{\mathbf{Y}}_0 dx + \int_0^L\int_0^x \exp\left[-\underline{\underline{\mathbf{A}}}\,(x-\lambda)\right]\underline{\mathbf{b}}d\lambda dx \tag{4.49}$$

Equation 4.49 can be rewritten as

$$\begin{bmatrix} \int_0^L \exp\left(-\underline{\underline{\mathbf{A}}}x\right)dx & -\underline{\underline{\mathbf{I}}} \end{bmatrix}\begin{bmatrix} \underline{\mathbf{Y}}_0 \\ \underline{\mathbf{Y}}_c \end{bmatrix} = -\int_0^L\int_0^x \exp\left[-\underline{\underline{\mathbf{A}}}\,(x-\lambda)\right]\underline{\mathbf{b}}d\lambda dx \tag{4.50}$$

Equation 4.42 becomes:

$$\begin{bmatrix} 0 & 1 \end{bmatrix}\underline{\mathbf{Y}}_0 = -\frac{i\left(1-t_+^0\right)}{DF} \tag{4.51}$$

Equation 4.43 becomes:

$$\begin{bmatrix} 1 & 0 \end{bmatrix}\underline{\mathbf{Y}}_c = c_b L \tag{4.52}$$

In this case $\underline{\underline{\mathbf{C}}} = \begin{bmatrix} 0 & 1 \\ 0 & 0 \end{bmatrix}$, $\underline{\underline{\mathbf{D}}} = \begin{bmatrix} 0 & 0 \\ 1 & 0 \end{bmatrix}$, and $\underline{\mathbf{Bc}} = \begin{bmatrix} -\frac{i\left(1-t_+^0\right)}{DF} \\ c_b L \end{bmatrix}$ Equation 4.51 and equation 4.52 put together become

$$\begin{bmatrix} \underline{\underline{\mathbf{C}}} & \underline{\underline{\mathbf{D}}} \end{bmatrix} \begin{bmatrix} \underline{\mathbf{Y}}_0 \\ \underline{\mathbf{Y}}_c \end{bmatrix} = \underline{\mathbf{Bc}} \tag{4.53}$$

From equation 4.50 and equation 4.53, the entire equation system can be expressed as:

$$\begin{bmatrix} \int_0^L \exp\left(-\underline{\underline{\mathbf{A}}}x\right) dx & -\underline{\underline{\mathbf{I}}} \\ \underline{\underline{\mathbf{C}}} & \underline{\underline{\mathbf{D}}} \end{bmatrix} \begin{bmatrix} \underline{\mathbf{Y}}_0 \\ \underline{\mathbf{Y}}_c \end{bmatrix} = \begin{bmatrix} -\int_0^L \int_0^x \exp\left[-\underline{\underline{\mathbf{A}}}\left(x-\lambda\right)\right] \underline{\mathbf{b}} d\lambda dx \\ \underline{\mathbf{Bc}} \end{bmatrix} \tag{4.54}$$

Let $\underline{\underline{\mathbf{M}}} = \begin{bmatrix} \int_0^L \exp\left(-\underline{\underline{\mathbf{A}}}x\right) dx & -\underline{\underline{\mathbf{I}}} \\ \underline{\underline{\mathbf{C}}} & \underline{\underline{\mathbf{D}}} \end{bmatrix}$, and $\underline{\mathbf{B}} = \begin{bmatrix} -\int_0^L \int_0^x \exp\left[-\underline{\underline{\mathbf{A}}}\left(x-\lambda\right)\right] \underline{\mathbf{b}} d\lambda dx \\ \underline{\mathbf{Bc}} \end{bmatrix}$, equation 4.54 can be simplified to

$$\underline{\underline{\mathbf{M}}} \begin{bmatrix} \underline{\mathbf{Y}}_0 \\ \underline{\mathbf{Y}}_c \end{bmatrix} = \underline{\mathbf{B}} \tag{4.55}$$

From equation 4.55

$$\begin{bmatrix} \underline{\mathbf{Y}}_0 \\ \underline{\mathbf{Y}}_c \end{bmatrix} = \underline{\underline{\mathbf{M}}}^{-1} \underline{\mathbf{B}} \tag{4.56}$$

$$\underline{\mathbf{Y}}_0 = \begin{bmatrix} \underline{\underline{\mathbf{I}}} & \underline{\underline{\mathbf{O}}} \end{bmatrix} \underline{\underline{\mathbf{M}}}^{-1} \underline{\mathbf{B}} \tag{4.57}$$

Substituting $\underline{\mathbf{Y}}_0$ from equation 4.57 into equation 4.48 gives

$$\underline{\mathbf{Y}} = \exp\left(-\underline{\underline{\mathbf{A}}}x\right) \begin{bmatrix} \underline{\underline{\mathbf{I}}} & \underline{\underline{\mathbf{O}}} \end{bmatrix} \underline{\underline{\mathbf{M}}}^{-1} \underline{\mathbf{B}} + \int_0^x \exp\left[-\underline{\underline{\mathbf{A}}}\left(x-\lambda\right)\right] \underline{\mathbf{b}} d\lambda \tag{4.58}$$

$$c = y_1 = \begin{bmatrix} 1 & 0 \end{bmatrix} \underline{\mathbf{Y}} = \begin{bmatrix} 1 & 0 \end{bmatrix} \exp\left(-\underline{\underline{\mathbf{A}}}x\right) \begin{bmatrix} \underline{\underline{\mathbf{I}}} & \underline{\underline{\mathbf{O}}} \end{bmatrix} \underline{\underline{\mathbf{M}}}^{-1} \underline{\mathbf{B}} + \int_0^x \exp\left[-\underline{\underline{\mathbf{A}}}\left(x-\lambda\right)\right] \underline{\mathbf{b}} d\lambda \tag{4.59}$$

The analytical solution obtained after the using the matrix exponential method is

$$c(x) = c_b + \frac{i(L-2x)\left(1-t_+^0\right)}{2DF} \tag{4.60}$$

Figure 4.4 shows the steady state concentration profile yielded by a matrix exponential method employing equations 4.41-4.43.

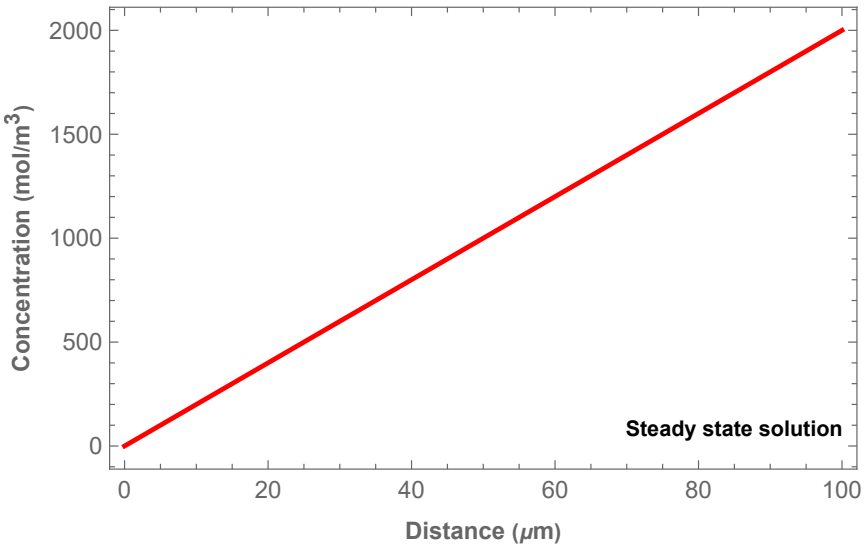

Figure 4.4: Steady state concentration profile in the galvanostatic cell by using method of exponential matrix.

Example 5: Doyle and Newman Simplified Model: Steady State Solutions

The extra constraint for this model [68] is the overall mass or mole balance (since no chemical reactions are occurring). This constraint can be derived based on the cross-sectional area, A (i.e., the projected area of the separator and electrode, see their Fig. 1) of the cell, the thickness of the separator, L_s, the thickness of the positive electrode, L_+, the porosities of the separator and the porous electrode (ϵ_s and ϵ, respectively), and the initial concentration, c_0 (moles per volume of pores filled with

electrolyte in the separator and the porous electrode):

$$A\int_0^{L_s}\epsilon_s c_0 dx + A\int_{L_s}^{L_s+L_+}\epsilon c_0 dx = Ac_0L_s\left(\epsilon_s + \epsilon\frac{L_+}{L_s}\right) \tag{4.61}$$

Note that it is necessary to find the volume of the separator and the volume of the porous electrode to find the total number of moles present initially in the separator and the porous electrode. The first term on the left hand side of equation 4.61 contains ϵ_s that represents the volume of the pores in the separator per volume of the separator, and the second term contains ϵ that represents the volume of the pores in the porous electrode per volume of the electrode. Note that equation 4.61 uses the initial concentration of the binary electrolyte, c_0, in the solution phase in the pores of both the separator and the porous cathode. In the separator $\epsilon_s c_0$ represents the moles per liter or cubic meter of the separator whereas in the porous electrode ϵc_0 represents the number of moles per liter in the porous electrode. Consequently, we multiply c_0 by the porosity (void volume per total volume of the porous electrode) to obtain the concentration per unit volume of the porous electrode, which is often called the superficial concentration [69]. The right hand side of equation 4.61 is the total number of moles present initially ($A\epsilon_s c_0 L_s$ moles in the separator and $A\epsilon c_0 L_+$ moles in the porous electrode). In this case [68], the separator is not porous. Consequently, $\epsilon_s = 1.0$, and we can think of the separator as being just a liquid reservoir of lithium ions and counter ions, and equation 4.61 becomes

$$A\int_0^{L_s} c_0 dx + A\int_{L_s}^{L_s+L_+}\epsilon c_0 dx = Ac_0L_s\left(1.0 + \epsilon\frac{L_+}{L_s}\right) \tag{4.62}$$

The total number of moles given on the right hand side of equation 4.62 will be conserved and redistributed during the electrochemical reactions that occur during the operation of the cell. For example, on discharge the lithium metal will be oxidized and lithium ions will enter the separator (reservoir) causing the average concentration of lithium ions and counter ions to go up, and at the same time lithium ions will be consumed in the porous electrode causing the average concentration of lithium ions

to go down in the porous electrode. Note that this will cause the anions in the porous electrode to move to the separator to maintain electroneutrality. However, we are using the concentration of the binary electrolyte in the pores as the dependent variable not the concentration of individual ions. It is worth noting that this model of a lithium battery is limited because the amount of lithium metal is assumed to be unlimited, and the porous electrode is assumed to be capable of acting as a sink for an unlimited amount of lithium ions. These assumptions are not realistic but provide a basis for gaining a better understanding of the concentration distribution in this cell. These assumptions provide the basis for obtaining a steady state solution for the concentration distribution, which is unrealistic for an actual cell. That is, a real battery does not have a steady state condition. Once a current is impressed on the lithium metal anode and the lithium ion consumption reaction occurs within the porous cathode, the following mole balance must apply:

$$A\int_0^{L_s} c_1(x,t)\,dx + A\int_{L_s}^{L_s+L_+} \epsilon c_2(x,t)\,dx = Ac_0L_s\left(1.0+\epsilon\frac{L_+}{L_s}\right) \tag{4.63}$$

where the subscripts 1 and 2 refer to the separator and the cathode, respectively. We can show that equation 4.63 must apply over time by integrating the governing equations and applying the boundary conditions. The governing equation in the separator is:

$$\frac{\partial c_1}{\partial t} = D\frac{\partial^2 c_1}{\partial x^2} \tag{4.64}$$

The first step is to integrate over x this material balance equation in the separator:

$$\int_0^{L_s}\frac{\partial c_1}{\partial t}dx = \int_0^{L_s} D\frac{\partial^2 c_1}{\partial x^2}dx = D\frac{\partial c_1}{\partial x}\bigg|_{x=L_s} - D\frac{\partial c_1}{\partial x}\bigg|_{x=0} \tag{4.65}$$

Let the number of moles in the separator be m_1:

$$m_1 = A\int_0^{L_s} c_1 dx \tag{4.66}$$

And let the number of moles in the porous electrode be m_2:

$$m_2 = A\int_{L_s}^{L_s+L_+} \epsilon c_2 dx \tag{4.67}$$

Equation 4.66 can be used to write Equation 4.65 as

$$\frac{\partial m_1}{\partial t} = AD\frac{\partial c_1}{\partial x}\bigg|_{x=L_s} - AD\frac{\partial c_1}{\partial x}\bigg|_{x=0} \tag{4.68}$$

The material balance for the porous electrode is an equation based concentrated solution theory and porous electrode theory [69]. The material equation for the x direction only is

$$\epsilon\frac{\partial c_2}{\partial t} = \epsilon^{3/2}D\frac{\partial^2 c_2}{\partial x^2} + aj_n\left(1 - t_+^0\right) \tag{4.69}$$

where we have assumed that

$$\frac{d\ln c_0}{d\ln c} = 0 \tag{4.70}$$

Integration of the material balance for the porous electrode with the pore wall flux, j_n, assumed to be a constant yields

$$\int_{x=L_s}^{x=L_s+L_+}\epsilon\frac{\partial c_2}{\partial t}dx = \int_{x=L_s}^{x=L_s+L_+}\left(\epsilon^{3/2}D\frac{\partial^2 c_2}{\partial x^2} + aj_n\left(1 - t_+^0\right)\right)dx$$

$$\int_{x=L_s}^{x=L_s+L_+}\epsilon\frac{\partial c_2}{\partial t}dx = D\epsilon^{3/2}\frac{\partial c_2}{\partial x}\bigg|_{x=L_s+L_+} - D\epsilon^{3/2}\frac{\partial c_2}{\partial x}\bigg|_{x=L_s} + aj_n\left(1 - t_+^0\right)(L_s + L_+ - L_s) \tag{4.71}$$

Equation 4.67 can be used to write equation 4.71 as

$$\frac{\partial m_2}{\partial t} = AD\epsilon^{3/2}\frac{\partial c_2}{\partial x}\bigg|_{x=L_s+L_+} - AD\epsilon^{3/2}\frac{\partial c_2}{\partial x}\bigg|_{x=L_s} + Aaj_n\left(1 - t_+^0\right)L_+ \tag{4.72}$$

The boundary condition at $x = 0$ can be written for our binary electrolyte as (see [69]):

$$\frac{AD}{(1 - t_+^0)}\frac{\partial c_1}{\partial x}\bigg|_{x=0} = -A\frac{I}{F} \tag{4.73}$$

where I is the current density based on the projected area of the electrode, A, D is the binary electrolyte diffusion coefficient, and t_+^0 is the cation transference number with respect to the solvent velocity. Substitution of equation 4.73 into equation 4.68 yields

$$\frac{\partial m_1}{\partial t} = AD\frac{\partial c_1}{\partial x}\bigg|_{x=L_s} + A\frac{I\left(1 - t_+^0\right)}{F} \tag{4.74}$$

The boundary condition at $x = L_s + L_+$ is as follows:

$$\left.\frac{\partial c_2}{\partial x}\right|_{x=L_s+L_+} = 0 \tag{4.75}$$

Substitution of equation 4.75 into equation 4.72 yields

$$\frac{\partial m_2}{\partial t} = -A\epsilon^{3/2} D \left.\frac{\partial c_2}{\partial x}\right|_{x=L_s} + Aaj_n \left(1 - t_+^0\right) L_+ \tag{4.76}$$

We now need to make the assumption that the pore wall flux of lithium ions, j_n, is simply related to the set current density, I:

$$j_n = -\frac{I}{aFL_+} \tag{4.77}$$

Substitution of equation 4.77 into equation 4.76 yields

$$\frac{\partial m_2}{\partial t} = -A\epsilon^{3/2} D \left.\frac{\partial c_2}{\partial x}\right|_{x=L_s} - A\frac{I\left(1 - t_+^0\right)}{F} \tag{4.78}$$

Addition of equations 4.74 and 4.78 yields

$$\frac{\partial \left(m_1 + m_2\right)}{\partial t} = AD \left.\frac{\partial c_1}{\partial x}\right|_{x=L_s} + A\frac{I\left(1 - t_+^0\right)}{F} - A\epsilon^{3/2} D \left.\frac{\partial c_2}{\partial x}\right|_{x=L_s} - A\frac{I\left(1 - t_+^0\right)}{F} \tag{4.79}$$

which reduces to

$$\frac{\partial \left(m_1 + m_2\right)}{\partial t} = AD \left.\frac{\partial c_1}{\partial x}\right|_{x=L_s} - A\epsilon^{3/2} D \left.\frac{\partial c_2}{\partial x}\right|_{x=L_s} \tag{4.80}$$

Finally, it is reasonable to require continuity of flux of the binary electrolyte from the separator to the porous electrode at $x = L_s$:

$$-\frac{D}{\left(1 - t_+^0\right)} \left.\frac{\partial c_1}{\partial x}\right|_{x=L_s} = -\frac{D\epsilon^{3/2}}{\left(1 - t_+^0\right)} \left.\frac{\partial c_2}{\partial x}\right|_{x=L_s} \tag{4.81}$$

which can be simplified and both sides multiplied by A to obtain

$$AD \left.\frac{\partial c_1}{\partial x}\right|_{x=L_s} = AD\epsilon^{3/2} \left.\frac{\partial c_2}{\partial x}\right|_{x=L_s} \tag{4.82}$$

Substitution of equation 4.82 into equation 4.80 shows that the total number of moles of the binary electrolyte in the separator and porous electrode $(m_1 + m_2)$ does not change with time:

$$\frac{\partial \left(m_1 + m_2\right)}{\partial t} = 0 \tag{4.83}$$

It is interesting to note that the constraint that the liquid phase concentrations be the same at $x = L_s$

$$c_1 = c_2 \quad \text{at} \quad x = L_s \tag{4.84}$$

is not required to obtain equation 4.83. However, it will be required to find the analytic solution to the model equations whereas equation 4.81 will not be needed as shown below. Equation 4.63 can be written in dimensionless form using the dimensionless variables:

$$\int_0^1 L_s \Theta_1 \left(X_1, \tau_1\right) dX_1 + \int_0^1 \epsilon L_+ \Theta_2 \left(X_2, \tau_2\right) dX_2 = L_s \left(1 + \epsilon \frac{L_+}{L_s}\right) \tag{4.85}$$

where:

$$\Theta_1 \left(X_1, \tau\right) = \frac{c_1}{c_0}, \Theta_2 \left(X_2, \tau\right) = \frac{c_2}{c_0}, X_1 = \frac{x}{L_s}, X_2 = \frac{x - L_s}{L_+},$$
$$\tau_1 = \frac{Dt}{L_s^2}, \tau_2 = \frac{Dt}{L_+^2}, J = \frac{a\left(1 - t_+^0\right) L_+^2 j_n}{\epsilon D c_0} \tag{4.86}$$

Note that at $\tau = 0$ the dimensionless concentrations are both equal to 1

$$\Theta_1 \left(X_1, 0\right) = \Theta_2 \left(X_2, 0\right) = 1 \quad \text{at} \quad \tau = 0 \tag{4.87}$$

Also note that for all time according to equation 4.84 we have continuity of the dependent variable at the interface between the separator and the porous electrode, which becomes in dimensionless form

$$\Theta_1 \left(1, \tau\right) = \Theta_2 \left(0, \tau\right) \tag{4.88}$$

Also note that once we start passing current from the lithium metal electrode into the separator, the dimensionless concentration will be greater than 1 in the separator, and the dimensionless concentration in the porous electrode will be less than ϵr. The reason this extra constraint is needed can be seen by solving the steady state model equations using the classical method. Substitution of the variables in equation 4.86 into equation 4.64 yields the dimensionless governing equation in the separator:

$$\frac{\partial \Theta_1}{\partial \tau} = \frac{\partial^2 \Theta_1}{\partial X_1^2} \tag{4.89}$$

Substitution of the variables in equation 4.86 into equation 4.69 yields the dimensionless governing equation in the porous electrode:

$$\frac{\partial \Theta_2}{\partial \tau} = \epsilon^{1/2} \frac{\partial^2 \Theta_2}{\partial X_2^2} + J \tag{4.90}$$

The boundary condition at $x = 0$ given by equation 4.73 becomes:

$$\left.\frac{\partial \Theta_1}{\partial X_1}\right|_{X_1=0} = -\gamma \quad \text{where} \quad \gamma = \frac{I\left(1 - t_+^0\right) L_s}{FDc_0} \tag{4.91}$$

Equation 4.75 becomes in dimensionless variables

$$\left.\frac{\partial \Theta_2}{\partial X_2}\right|_{X_2=1} = 0 \tag{4.92}$$

The continuity of flux from the separator to the porous electrode given in equation 4.81 becomes in dimensionless form

$$\left.\frac{1}{L_s}\frac{\partial \Theta_1}{\partial X_1}\right|_{X_1=1} = \left.\frac{\epsilon^{3/2}}{L_+}\frac{\partial \Theta_2}{\partial X_2}\right|_{X_2=0} \tag{4.93}$$

X_1 and X_2 are independent variables that can be replaced by a single dummy variable x then equations. Let $y_1 = \Theta_1$, $y_2 = \Theta_2$, $y_3 = \frac{d\Theta_1}{dx}$, and $y_4 = \frac{d\Theta_2}{dx}$ and at steady state the governing equations 4.89 and 4.90 become the following system of equations

$$\frac{dy_1}{dx} = y_3 \tag{4.94}$$

$$\frac{dy_2}{dx} = y_4 \tag{4.95}$$

$$\frac{dy_3}{dx} = 0 \tag{4.96}$$

$$\frac{dy_4}{dx} = -\frac{J}{\epsilon^{1/2}} \tag{4.97}$$

Rewrite equations 4.94, 4.95, 4.96, and 4.97

$$\frac{d}{dx}\begin{bmatrix} y_1 \\ y_2 \\ y_3 \\ y_4 \end{bmatrix} + \begin{bmatrix} 0 & 0 & -1 & 0 \\ 0 & 0 & 0 & -1 \\ 0 & 0 & 0 & 0 \\ 0 & 0 & 0 & 0 \end{bmatrix} \begin{bmatrix} y_1 \\ y_2 \\ y_3 \\ y_4 \end{bmatrix} = \begin{bmatrix} 0 \\ 0 \\ 0 \\ -\frac{J}{\epsilon^{1/2}} \end{bmatrix} \tag{4.98}$$

Let $\underline{\mathbf{Y}} = \begin{bmatrix} y_1 \\ y_2 \\ y_3 \\ y_4 \end{bmatrix}$, $\underline{\underline{\mathbf{A}}} = \begin{bmatrix} 0 & 0 & -1 & 0 \\ 0 & 0 & 0 & -1 \\ 0 & 0 & 0 & 0 \\ 0 & 0 & 0 & 0 \end{bmatrix}$, and $\underline{\mathbf{b}} = \begin{bmatrix} 0 \\ 0 \\ 0 \\ -\frac{J}{\epsilon^{1/2}} \end{bmatrix}$, the equation system can be expressed with the matrix format

$$\frac{d\underline{\mathbf{Y}}}{dx} + \underline{\underline{\mathbf{A}}}\ \underline{\mathbf{Y}} = \underline{\mathbf{b}} \tag{4.99}$$

The general form of the solution is obtained from equation 4.99

$$\underline{\mathbf{Y}} = \exp\left(-\underline{\underline{\mathbf{A}}}x\right)\underline{\mathbf{Y}}_0 + \int_0^x \exp\left[-\underline{\underline{\mathbf{A}}}\,(x-\lambda)\right]\underline{\mathbf{b}}\,(\lambda)\,d\lambda \tag{4.100}$$

Let $\underline{\mathbf{Y}}_0 = \underline{\mathbf{Y}}|_{x=0}$, $\underline{\mathbf{Y}}_1 = \underline{\mathbf{Y}}|_{x=1}$ and $\underline{\mathbf{Y}}_c = \int_0^1 \underline{\mathbf{Y}}dx$ and obtain

$$\underline{\mathbf{Y}}_1 = \exp\left(-\underline{\underline{\mathbf{A}}}x\right)\underline{\mathbf{Y}}_0 + \int_0^1 \exp\left[-\underline{\underline{\mathbf{A}}}\,(1-t)\right]\underline{\mathbf{b}}\,(\lambda)\,d\lambda \tag{4.101}$$

$$\underline{\mathbf{Y}}_c = \int_0^1 \underline{\mathbf{Y}}dx = \int_0^1 \exp\left(-\underline{\underline{\mathbf{A}}}x\right)\underline{\mathbf{Y}}_0 dx + \int_0^1\int_0^x \exp\left[-\underline{\underline{\mathbf{A}}}\,(x-\lambda)\right]\underline{\mathbf{b}}\,(\lambda)\,d\lambda dx \tag{4.102}$$

Equations 4.101 and 4.102 are rewritten as

$$\begin{bmatrix} \exp\left(-\underline{\underline{\mathbf{A}}}\right) & -\underline{\underline{\mathbf{I}}} & \underline{\underline{\mathbf{O}}} \\ \int_0^1 \exp\left(-\underline{\underline{\mathbf{A}}}x\right)dx & \underline{\underline{\mathbf{O}}} & -\underline{\underline{\mathbf{I}}} \end{bmatrix} \begin{bmatrix} \underline{\mathbf{Y}}_0 \\ \underline{\mathbf{Y}}_1 \\ \underline{\mathbf{Y}}_c \end{bmatrix} = \begin{bmatrix} -\int_0^1 \exp\left[-\underline{\underline{\mathbf{A}}}\,(1-\lambda)\right]\underline{\mathbf{b}}d\lambda \\ -\int_0^1\int_0^x \exp\left[-\underline{\underline{\mathbf{A}}}\,(x-\lambda)\right]\underline{\mathbf{b}}d\lambda dx \end{bmatrix} \tag{4.103}$$

Equation 4.91 and equation 4.88 are expressed as:

$$\begin{bmatrix} 0 & 0 & 1 & 0 \\ 0 & 1 & 0 & 0 \end{bmatrix} \underline{\mathbf{Y}}_0 = \begin{bmatrix} -\gamma \\ 0 \end{bmatrix} \tag{4.104}$$

Equation 4.91 and equation 4.88 are expressed as:

$$\begin{bmatrix} -1 & 0 & 0 & 0 \\ 0 & 0 & 0 & 1 \end{bmatrix} \underline{\mathbf{Y}}_1 = \begin{bmatrix} 0 \\ 0 \end{bmatrix} \tag{4.105}$$

Equation 4.85 is expressed as:

$$\begin{bmatrix} L_s & \epsilon L_+ & 0 & 0 \end{bmatrix} \underline{\mathbf{Y}}_c = L_s\left(1 + \epsilon\frac{L_+}{L_s}\right) \tag{4.106}$$

Let $\underline{\underline{\mathbf{C}}} = \begin{bmatrix} 0 & 0 & 1 & 0 \\ 0 & 1 & 0 & 0 \\ 0 & 0 & 0 & 0 \\ 0 & 0 & 0 & 0 \end{bmatrix}$, $\underline{\underline{\mathbf{D}}} = \begin{bmatrix} 0 & 0 & 0 & 0 \\ -1 & 0 & 0 & 0 \\ 0 & 0 & 0 & 1 \\ 0 & 0 & 0 & 0 \end{bmatrix}$, $\underline{\underline{\mathbf{E}}} = \begin{bmatrix} 0 & 0 & 0 & 0 \\ 0 & 0 & 0 & 0 \\ 0 & 0 & 0 & 0 \\ L_s & \epsilon L_+ & 0 & 0 \end{bmatrix}$, and $\underline{\mathbf{Bc}} = \begin{bmatrix} -\gamma \\ 0 \\ 0 \\ L_s\left(1+\epsilon\frac{L_+}{L_s}\right) \end{bmatrix}$ Equations 4.104, 4.105 and 4.106 be put together

$$\begin{bmatrix} \underline{\underline{\mathbf{C}}} & \underline{\underline{\mathbf{D}}} & \underline{\underline{\mathbf{E}}} \end{bmatrix} \begin{bmatrix} \underline{\mathbf{Y}}_0 \\ \underline{\mathbf{Y}}_1 \\ \underline{\mathbf{Y}}_c \end{bmatrix} = \underline{\mathbf{Bc}} \tag{4.107}$$

From equation 4.103 and equation 4.107, the entire equation system is expressed as:

$$\begin{bmatrix} \exp\left(-\underline{\underline{\mathbf{A}}}\right) & -\underline{\underline{\mathbf{I}}} & \underline{\underline{\mathbf{O}}} \\ \int_0^1 \exp\left(-\underline{\underline{\mathbf{A}}}x\right) dx & \underline{\underline{\mathbf{O}}} & -\underline{\underline{\mathbf{I}}} \\ \underline{\underline{\mathbf{C}}} & \underline{\underline{\mathbf{D}}} & \underline{\underline{\mathbf{E}}} \end{bmatrix} \begin{bmatrix} \underline{\mathbf{Y}}_0 \\ \underline{\mathbf{Y}}_1 \\ \underline{\mathbf{Y}}_c \end{bmatrix} = \begin{bmatrix} -\int_0^1 \exp\left[-\underline{\underline{\mathbf{A}}}(1-\lambda)\right] \underline{\mathbf{b}}(\lambda)\, d\lambda \\ -\int_0^1 \int_0^x \exp\left[-\underline{\underline{\mathbf{A}}}(x-\lambda)\right] \underline{\mathbf{b}}(\lambda)\, d\lambda dx \\ \underline{\mathbf{Bc}} \end{bmatrix} \tag{4.108}$$

Let $\underline{\underline{\mathbf{M}}} = \begin{bmatrix} \exp\left(-\underline{\underline{\mathbf{A}}}\right) & -\underline{\underline{\mathbf{I}}} & \underline{\underline{\mathbf{O}}} \\ \int_0^1 \exp\left(-\underline{\underline{\mathbf{A}}}x\right) dx & \underline{\underline{\mathbf{O}}} & -\underline{\underline{\mathbf{I}}} \\ \underline{\underline{\mathbf{C}}} & \underline{\underline{\mathbf{D}}} & \underline{\underline{\mathbf{E}}} \end{bmatrix}$, and $\underline{\mathbf{B}} = \begin{bmatrix} -\int_0^1 \exp\left[-\underline{\underline{\mathbf{A}}}(1-\lambda)\right] \underline{\mathbf{b}}(\lambda)\, d\lambda \\ -\int_0^1 \int_0^x \exp\left[-\underline{\underline{\mathbf{A}}}(x-\lambda)\right] \underline{\mathbf{b}}(\lambda)\, d\lambda dx \\ \underline{\mathbf{Bc}} \end{bmatrix}$, equation 4.108 is simplified as

$$\underline{\underline{\mathbf{M}}} \begin{bmatrix} \underline{\mathbf{Y}}_0 \\ \underline{\mathbf{Y}}_1 \\ \underline{\mathbf{Y}}_c \end{bmatrix} = \underline{\mathbf{B}} \tag{4.109}$$

From equation 4.109

$$\begin{bmatrix} \underline{\mathbf{Y}}_0 \\ \underline{\mathbf{Y}}_1 \\ \underline{\mathbf{Y}}_c \end{bmatrix} = \underline{\underline{\mathbf{M}}}^{-1}\underline{\mathbf{B}} \tag{4.110}$$

$$\underline{\mathbf{Y}}_0 = \begin{bmatrix} \underline{\underline{\mathbf{I}}} & \underline{\underline{\mathbf{O}}} & \underline{\underline{\mathbf{O}}} \end{bmatrix} \underline{\underline{\mathbf{M}}}^{-1}\underline{\mathbf{B}} \tag{4.111}$$

Substituting $\underline{\mathbf{Y}}_0$ from equation 4.111 in equation 4.100 gives

$$\underline{\mathbf{Y}} = \exp\left(-\underline{\underline{\mathbf{A}}}x\right) \begin{bmatrix} \underline{\underline{\mathbf{I}}} & \underline{\underline{\mathbf{O}}} & \underline{\underline{\mathbf{O}}} \end{bmatrix} \underline{\underline{\mathbf{M}}}^{-1}\underline{\mathbf{B}} + \int_0^x \exp\left[-\underline{\underline{\mathbf{A}}}\left(x-\lambda\right)\right] \underline{\mathbf{b}} d\lambda \tag{4.112}$$

$$\Theta_1 = \begin{bmatrix} 1 & 0 & 0 & 0 \end{bmatrix} \underline{\mathbf{Y}} = \begin{bmatrix} 1 & 0 & 0 & 0 \end{bmatrix} \exp\left(-\underline{\underline{\mathbf{A}}}x\right) \begin{bmatrix} \underline{\underline{\mathbf{I}}} & \underline{\underline{\mathbf{O}}} & \underline{\underline{\mathbf{O}}} \end{bmatrix} \underline{\underline{\mathbf{M}}}^{-1}\underline{\mathbf{B}} + \int_0^x \exp\left[-\underline{\underline{\mathbf{A}}}\left(x-\lambda\right)\right] \underline{\mathbf{b}} d\lambda \tag{4.113}$$

$$\Theta_2 = \begin{bmatrix} 0 & 1 & 0 & 0 \end{bmatrix} \underline{\mathbf{Y}} = \begin{bmatrix} 0 & 1 & 0 & 0 \end{bmatrix} \exp\left(-\underline{\underline{\mathbf{A}}}x\right) \begin{bmatrix} \underline{\underline{\mathbf{I}}} & \underline{\underline{\mathbf{O}}} & \underline{\underline{\mathbf{O}}} \end{bmatrix} \underline{\underline{\mathbf{M}}}^{-1}\underline{\mathbf{B}} + \int_0^x \exp\left[-\underline{\underline{\mathbf{A}}}\left(x-\lambda\right)\right] \underline{\mathbf{b}} d\lambda \tag{4.114}$$

Thus, the dimensionless concentration profiles obtained using Maple are

$$\Theta_1 = -\frac{JL_+\sqrt{\epsilon}}{3\left(\epsilon L_+ + L_s\right)} + \frac{\left(2\epsilon L_+ + L_s\right)\gamma}{2\left(\epsilon L_+ + L_s\right)} + \frac{L_s\left(1+\epsilon\frac{L_+}{L_s}\right)}{\epsilon L_+ + L_s} - x\gamma \tag{4.115}$$

$$\Theta_2 = -\frac{JL_+\sqrt{\epsilon}}{3\left(\epsilon L_+ + L_s\right)} - \frac{L_s\gamma}{2\left(\epsilon L_+ + L_s\right)} + \frac{L_s\left(1+\epsilon\frac{L_+}{L_s}\right)}{\epsilon L_+ + L_s} + \frac{\left(x-1\right)J}{\sqrt{\epsilon}r} - \frac{\left(x-1\right)^2 J}{2\sqrt{\epsilon}r^2} \tag{4.116}$$

These equations are the same as Eqs. 17 and 18 of Doyle and Newman [68] with necessary sign changes for their equations. That is, the second minus sign in their Eq. 19 needs to be changed to a plus sign, and the first minus sign in their Eq. 20 needs to be changed to a plus sign. Steady state concentration profiles at various current densities for the model system described above and the comparison with COMSOL solutions are given in Figure 4.5.

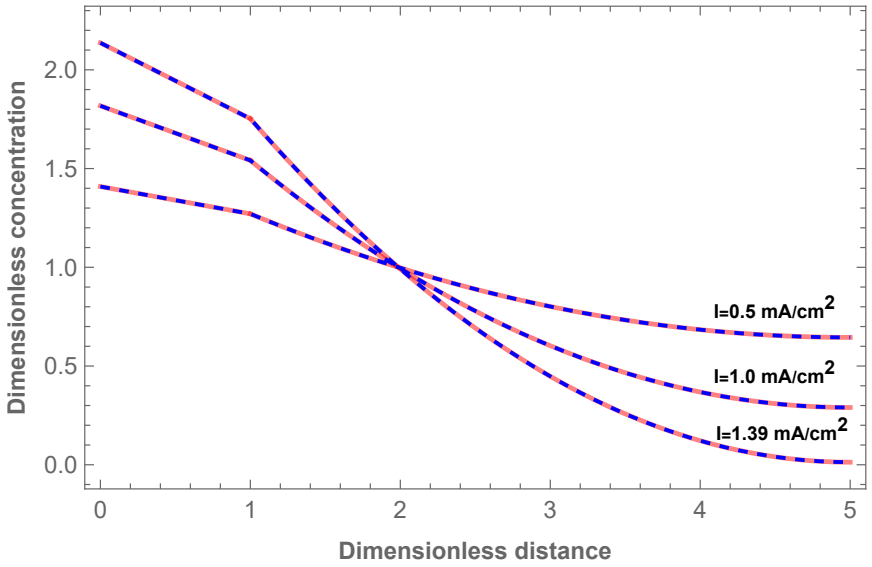

Figure 4.5: Comparison of steady state concentration profiles across the full cell for galvanostatic discharges at various current densities by using method of exponential matrix and COMSOL.

4.4 Conclusions

An analytic solution method has been presented for solving single or multiple dependent variable second-order linear BVPs in single and multiple domains. The presented method is straightforward and provides a general solution, valid for different boundary conditions and constraints. Furthermore, the method can solve nonlinear and time-dependent problems using the semi-analytic technique [70] and [71]. Maple worksheets used for obtaining the results in this paper are available upon request from the authors.

Bibliography

[1] Research and M. ltd. Lithium-ion battery market by type (lithium nickel manganese cobalt oxide (li-nmc), lithium iron phosphate (lfp), lithium cobalt oxide (lco)), capacity, voltage, industry (consumer electronics, automotive, aerospace) - global forecast to 2031. 2022.

[2] Doron Aurbach, Yair Ein-Eli, Boris Markovsky, Arie Zaban, S Luski, Y Carmeli, and H Yamin. The study of electrolyte solutions based on ethylene and diethyl carbonates for rechargeable li batteries: Ii. graphite electrodes. Journal of The Electrochemical Society, 142(9):2882, 1995.

[3] Dong H Jang, Young J Shin, and Seung M Oh. Dissolution of spinel oxides and capacity losses in 4 v li/li x mn2 o 4 cells. Journal of The Electrochemical Society, 143(7):2204, 1996.

[4] Emanuel Peled. The electrochemical behavior of alkali and alkaline earth metals in nonaqueous battery systems - the solid electrolyte interphase model. Journal of The Electrochemical Society, 126(12):2047, 1979.

[5] TR Ashwin, Andrew McGordon, Widanalage Dhammika Widanage, and Paul A Jennings. Modified electrochemical parameter estimation of ncr18650bd battery using implicit finite volume method. Journal of Power Sources, 341:387–395, 2017.

[6] MICHEL Broussely, S Herreyre, Ph Biensan, P Kasztejna, K Nechev, and RJ Staniewicz. Aging mechanism in li ion cells and calendar life predictions. Journal of Power Sources, 97:13–21, 2001.

[7] John Christensen and John Newman. A mathematical model for the lithium-ion negative electrode solid electrolyte interphase. Journal of The Electrochemical Society, 151(11):A1977, 2004.

[8] Andrew M Colclasure, Kandler A Smith, and Robert J Kee. Modeling detailed chemistry and transport for solid-electrolyte-interface (sei) films in li–ion batteries. Electrochimica Acta, 58:33–43, 2011.

[9] C Delacourt and M Safari. Life simulation of a graphite/lifepo4 cell under cycling and storage. Journal of The Electrochemical Society, 159(8):A1283, 2012.

[10] Abhishek Deshpande, Saksham Phul, and Balaji Krishnamurthy. A generalized mathematical model to understand the capacity fading in lithium ion batteries-effects of solvent and lithium transport. Journal of Electrochemical Science and Engineering, 5(3):181–195, 2015.

[11] Rujian Fu, Song-Yul Choe, Victor Agubra, and Jeffrey Fergus. Development of a physics-based degradation model for lithium ion polymer batteries considering side reactions. Journal of Power Sources, 278:506–521, 2015.

[12] Xing Jin, Ashish Vora, Vaidehi Hoshing, Tridib Saha, Gregory Shaver, R Edwin García, Oleg Wasynczuk, and Subbarao Varigonda. Physically-based reduced-order capacity loss model for graphite anodes in li-ion battery cells. Journal of Power Sources, 342:750–761, 2017.

[13] Niloofar Kamyab, John W Weidner, and Ralph E White. Mixed mode growth model for the solid electrolyte interface (sei). Journal of The Electrochemical Society, 166(2):A334, 2019.

[14] Andrea Lamorgese, Roberto Mauri, and Bernardo Tellini. Electrochemical-thermal p2d aging model of a licoo2/graphite cell: Capacity fade simulations. Journal of Energy Storage, 20:289–297, 2018.

[15] Jong-Won Lee, Yogesh K Anguchamy, and Branko N Popov. Simulation of charge–discharge cycling of lithium-ion batteries under low-earth-orbit conditions. Journal of Power Sources, 162(2):1395–1400, 2006.

[16] Xianke Lin, Jonghyun Park, Lin Liu, Yoonkoo Lee, AM Sastry, and Wei Lu. A comprehensive capacity fade model and analysis for li-ion batteries. Journal of The Electrochemical Society, 160(10):A1701, 2013.

[17] Lin Liu, Jonghyun Park, Xianke Lin, Ann Marie Sastry, and Wei Lu. A thermal-electrochemical model that gives spatial-dependent growth of solid electrolyte interphase in a li-ion battery. Journal of power sources, 268:482–490, 2014.

[18] Gang Ning and Branko N Popov. Cycle life modeling of lithium-ion batteries. Journal of The Electrochemical Society, 151(10):A1584, 2004.

[19] Saksham Phul, Abhishek Deshpande, and Balaji Krishnamurthy. A mathematical model to study the effect of potential drop across the sei layer on the capacity fading of a lithium ion battery. Electrochimica Acta, 164:281–287, 2015.

[20] Matthew B Pinson and Martin Z Bazant. Theory of sei formation in rechargeable batteries: capacity fade, accelerated aging and lifetime prediction. Journal of the Electrochemical Society, 160(2):A243, 2012.

[21] Harry J Ploehn, Premanand Ramadass, and Ralph E White. Solvent diffusion model for aging of lithium-ion battery cells. Journal of The Electrochemical Society, 151(3):A456, 2004.

[22] Githin K Prasad and Christopher D Rahn. Model based identification of aging parameters in lithium ion batteries. Journal of power sources, 232:79–85, 2013.

[23] Saeed Khaleghi Rahimian, Mehdi M Forouzan, Sangwoo Han, and Yifan Tang. A generalized physics-based calendar life model for li-ion cells. Electrochimica Acta, 348:136343, 2020.

[24] P Ramadass, Bala Haran, Parthasarathy M Gomadam, Ralph White, and Branko N Popov. Development of first principles capacity fade model for li-ion cells. Journal of the Electrochemical Society, 151(2):A196, 2004.

[25] Ramaraja P Ramasamy, Jong-Won Lee, and Branko N Popov. Simulation of capacity loss in carbon electrode for lithium-ion cells during storage. Journal of power sources, 166(1):266–272, 2007.

[26] M Safari and C Delacourt. Simulation-based analysis of aging phenomena in a commercial graphite/lifepo4 cell. Journal of The Electrochemical Society, 158(12):A1436, 2011.

[27] M Safari, M Morcrette, A Teyssot, and C Delacourt. Multimodal physics-based aging model for life prediction of li-ion batteries. Journal of The Electrochemical Society, 156(3):A145, 2008.

[28] Shrihari Sankarasubramanian and Balaji Krishnamurthy. A capacity fade model for lithium-ion batteries including diffusion and kinetics. Electrochimica Acta, 70:248–254, 2012.

[29] Shriram Santhanagopalan, Qingzhi Guo, Premanand Ramadass, and Ralph E White. Review of models for predicting the cycling performance of lithium ion batteries. Journal of power sources, 156(2):620–628, 2006.

[30] Siqi Shi, Peng Lu, Zhongyi Liu, Yue Qi, Louis G Hector Jr, Hong Li, and Stephen J Harris. Direct calculation of li-ion transport in the solid electrolyte interphase. Journal of the American Chemical Society, 134(37):15476–15487, 2012.

[31] Xiao-Guang Yang, Yongjun Leng, Guangsheng Zhang, Shanhai Ge, and Chao-Yang Wang. Modeling of lithium plating induced aging of lithium-ion batteries: Transition from linear to nonlinear aging. Journal of Power Sources, 360:28–40, 2017.

[32] Tetsuya Osaka, Toshiyuki Momma, Daikichi Mukoyama, and Hiroki Nara. Proposal of novel equivalent circuit for electrochemical impedance analysis of commercially available lithium ion battery. Journal of Power Sources, 205:483–486, 2012.

[33] Qi Zhang and Ralph E White. Capacity fade analysis of a lithium ion cell. Journal of Power Sources, 179(2):793–798, 2008.

[34] Yinyin Zhao, Song-Yul Choe, and Jungdo Kee. Modeling of degradation effects and its integration into electrochemical reduced order model for li (mn-nico) o2/graphite polymer battery for real time applications. Electrochimica Acta, 270:440–452, 2018.

[35] Mehdi Chouchane, Oier Arcelus, and Alejandro A Franco. Heterogeneous solid-electrolyte interphase in graphite electrodes assessed by 4d-resolved computational simulations. Batteries & Supercaps, 4(9):1457–1463, 2021.

[36] Supratim Das, Peter M Attia, William C Chueh, and Martin Z Bazant. Electrochemical kinetics of sei growth on carbon black: Part ii. modeling. Journal of The Electrochemical Society, 166(4):E107, 2019.

[37] Maureen Tang, Sida Lu, and John Newman. Experimental and theoretical investigation of solid-electrolyte-interphase formation mechanisms on glassy carbon. Journal of the Electrochemical Society, 159(11):A1775, 2012.

[38] Dongjiang Li, Dmitry Danilov, Zhongru Zhang, Huixin Chen, Yong Yang, and Peter HL Notten. Modeling the sei-formation on graphite electrodes in lifepo4 batteries. Journal of The Electrochemical Society, 162(6):A858, 2015.

[39] Ramaraja P Ramasamy, P Ramadass, Bala S Haran, and Branko N Popov. Synthesis, characterization and cycling performance of novel chromium oxide

cathode materials for lithium batteries. Journal of power sources, 124(1):155–162, 2003.

[40] Ramaraja P Ramasamy, Ralph E White, and Branko N Popov. Calendar life performance of pouch lithium-ion cells. Journal of Power Sources, 141(2):298–306, 2005.

[41] Peter M Attia, William C Chueh, and Stephen J Harris. Revisiting the t0. 5 dependence of sei growth. Journal of the Electrochemical Society, 167(9):090535, 2020.

[42] Michel Broussely, Ph Biensan, F Bonhomme, Ph Blanchard, S Herreyre, K Nechev, and RJ Staniewicz. Main aging mechanisms in li ion batteries. Journal of power sources, 146(1-2):90–96, 2005.

[43] Kyungmi Lim, Bernhard Fenk, Jelena Popovic, and Joachim Maier. Porosity of solid electrolyte interphases on alkali metal electrodes with liquid electrolytes. ACS applied materials & interfaces, 13(43):51767–51774, 2021.

[44] Jelena Popovic. Solid electrolyte interphase growth on mg metal anode: Case study of glyme-based electrolytes. Energy Technology, 9(4):2001056, 2021.

[45] Selcuk Atalay, Muhammad Sheikh, Alessandro Mariani, Yu Merla, Ed Bower, and W Dhammika Widanage. Theory of battery ageing in a lithium-ion battery: Capacity fade, nonlinear ageing and lifetime prediction. Journal of Power Sources, 478:229026, 2020.

[46] Ruihe Li, Simon OKane, Monica Marinescu, and Gregory J Offer. Modelling solvent consumption from sei layer growth in lithium-ion batteries. Journal of The Electrochemical Society, 169(6):060516, 2022.

[47] Robert Darling and John Newman. Modeling side reactions in composite li y mn2 o 4 electrodes. Journal of The Electrochemical Society, 145(3):990, 1998.

[48] Alkis Constantinides and Navid Mostoufi. Numerical Methods for Chemical Engineers with MATLAB Applications with Cdrom. Prentice Hall PTR, 1999.

[49] Jaroslav Heyrovsky. XXIX. Electrolysis with a dropping mercury cathode. Part I. Deposition of alkali and alkaline earth metals. Philosophical Magazine, 45(266):303–315, 1923.

[50] Dionyz Ilkovic. Polarographic Studies with the Dropping Mercury Kathode. Part XLIV. The Dependence of Limiting Currents on the Diffusion Constant, on the Rate of Dropping, and on the Size of Drops. Collection of Czechoslovak Chemical Communications, 6:498–513, 1934.

[51] Dionyz Ilkovic. Sur la valeur des courants de diffusion observés dans l'électrolyse à l'aide de l'électrode à gouttes de mercure. Ètude polarographique. Journal de Chimie Physique, 35:129–135, 1938.

[52] D. MacGillavry and E. K. Rideal. On the theory of limiting currents. I. Polarographic limiting currents. Recueil des Travaux Chimiques des Pays-Bas, 56(10):1013–1021, 1937.

[53] Jaroslav Koutecky. Correction for spherical diffusion to the Ilkovic equation. Czechoslovak Journal of Physics, 2:50–54, 1953.

[54] V. G. Levich. Physicochemical Hydrodynamics. Prentice-Hall, Englewood Cliffs, New Jersey, 1962.

[55] John Newman. Note. The Koutecky correction to the Ilkovic equation. Journal of Electroanalytical Chemistry and Interfacial Electrochemistry, 15:309–312, 1967.

[56] Zdenek Samec. History of the Ilkovic equation. Review of Polarography, 48(3):200–203, 2002.

[57] Eric W Weisstein. CRC concise encyclopedia of mathematics. Chapman and Hall/CRC, 2002.

[58] F. Rathgeber, D. A. Ham, L. Mitchell, M. Lange, F. Luporini, A. T. T. McRae, G. Bercea, G. R. Markall, and P. H. J. Kelly. Firedrake: Automating the finite element method by composing abstractions. ACM Transactions on Mathematical Software (TOMS), 43(3):1–27, 2016.

[59] P. R. Amestoy, I. S. Duff, L'Excellent J.-Y., and J. Koster. A fully asynchronous multifrontal solver using distributed dynamic scheduling. SIAM Journal on Matrix Analysis and Applications, 23(1):15–41, 2001.

[60] P. R. Amestoy, A. Guermouche, J.-Y. L'Excellent, and S. Pralet. Hybrid scheduling for the parallel solution of linear systems. Parallel Computing, 32(2):136–156, 2006.

[61] S. Balay, S. Abhyankar, M. F. Adams, J. Brown, P. Brune, K. Buschelman, L. Dalcin, V. Eijkhout, W. D. Gropp, D. Karpeyev, D. Kaushik, M. G. Knepley, D. May, L. C. McInnes, R. T. Mills, T. Munson, K. Rupp, P. Sanan, B. F. Smith, S. Zampini, H. Zhang, and H. Zhang. PETSc users manual. Technical Report ANL-95/11 - Revision 3.11, 2019.

[62] S. Balay, W. D. Gropp, L. C. McInnes, and B. F. Smith. Efficient management of parallelism in object oriented numerical software libraries. In E. Arge, A. M. Bruaset, and H. P. Langtangen, editors, Modern Software Tools in Scientific Computing, pages 163–202. Birkhäuser Press, 1997.

[63] Richard G Rice and Duong D Do. Applied mathematics and modeling for chemical engineers. John Wiley & Sons, 2012.

[64] A Varma and M Morbidelli. Oxford university press; new york: 1997. Mathematical Methods in Chemical Engineering, 1997.

[65] Venkat R Subramanian and Ralph E White. Solving differential equations with maple. Chemical Engineering Education, 34(4):328–336, 2000.

[66] W. M. Deen. Analysis of Transport Phenomena, 2nd ed. Oxford University Press, New York, 2012.

[67] Charles Monroe and John Newman. Dendrite growth in lithium/polymer systems: A propagation model for liquid electrolytes under galvanostatic conditions. Journal of The Electrochemical Society, 150(10):A1377, 2003.

[68] Marc Doyle and John Newman. Analysis of capacity–rate data for lithium batteries using simplified models of the discharge process. Journal of Applied Electrochemistry, 27(7):846–856, 1997.

[69] John Newman and Karen E Thomas-Alyea. Electrochemical systems. John Wiley & Sons, 2012.

[70] P De Vidts and Ralph E White. A semi-analytical solution method for linear partial differential equations. Computers & chemical engineering, 16(10-11):1007–1009, 1992.

[71] Venkat R Subramanian and Ralph E White. A semianalytical method for predicting primary and secondary current density distributions: Linear and nonlinear boundary conditions. Journal of the Electrochemical Society, 147(5):1636, 2000.